



Eidgenössische Technische Hochschule Zürich  
Swiss Federal Institute of Technology Zurich



Institut für Werkzeugmaschinen und Fertigung  
Institute of Machine Tools and Manufacturing

# **Development of a Low-Cost Modal Analysis System**

Roman Rüttimann

Master Thesis

Nino Ceresa  
Prof. Konrad Wegener

Institute of Machine Tools and Manufacturing



# **Abstract**

Experimental modal analysis in tandem with the modal model of a machine tool is a powerful procedure for the evaluation of the machine tools' dynamic behavior. But because experimental modal analysis is an expensive procedure, both due to high instrument costs and the need for experienced operators, the modal model is often not verified.

With the aim to decrease instrument costs and increase the use of experimental modal analysis, the system presented in this thesis consists of a micro controller based data acquisition system, a modal impact hammer and a low-cost accelerometer. The latter is a capacitive micro-electro-mechanical-sensor and the impact hammer is using a strain gauge load cell as impact sensor.

For the implementation of a low-cost modal analysis system based on the aforementioned components a micro controller based bus system and a specialized communication protocol is suggested.



# **Zusammenfassung**

Die experimentelle Modalanalyse, in Kombination mit dem modalen Modell einer Werkzeugmaschine, ist ein mächtiges Verfahren, um das dynamische Verhalten der Werkzeugmaschine zu evaluieren. Teure Messinstrumente und der Bedarf an erfahrenen Bedienern machen die experimentelle Modalanalyse allerdings zu einem kostspieligen Unterfangen. Oft wird daher das modale Modell gar nicht validiert.

Mit dem Ziel die Kosten für Messinstrumente zu senken und den Gebrauch von experimenteller Modalanalyse zu steigern, wird in dieser Arbeit ein System vorgestellt, welches aus einem Mikrokontroller-basierten Datenakquisitionssystem, einem Impulshammer und einem kostengünstigen Beschleunigungssensor besteht. Letzterer ist ein kapazitiver mikro-elektronisch-mechanischer Sensor und der Impulshammer ist mit einer Dehnmessstreifen basierten Ladungszelle ausgestattet.

Für die Umsetzung eines kostengünstigen Modalanalysesystems auf der Grundlage der zuvor genannten Komponenten, wird ein Mikrokontroller-basiertes Bus-System mit einem spezialisierten Kommunikationsprotokoll vorgeschlagen.



# Entwicklung eines Low-cost-Modalanalyse-Systems

Bachelor- / Masterarbeit

---

## **Problemstellung**

Mit zunehmender Verbreitung von simulationsgestützter Entwicklung wird auch der Bedarf nach Methoden zur Modellverifikation in der Industrie grösser. Die experimentelle Modalanalyse (EMA) ist ein mächtiges Werkzeug zur Validierung von Simulationsmodellen von Werkzeugmaschinen. Dabei wird die Struktur mittels Impulshammer angeregt und die Antwort mit Beschleunigungssensoren gemessen. Kommerziell erhältliche EMA-Systeme kosten jedoch schnell über 50'000 CHF und sind daher für die breite Anwendung nicht geeignet. Für die Modellvalidierung sind jedoch die Auflösung und die Abtastrate des Messsystems häufig weniger kritisch, was den Einsatz von günstigeren Komponenten zulassen würde.

Mit den heute erhältlichen MEMS-Beschleunigungssensoren (wie sie in jedem Smartphone verbaut werden) und Mikrocontroller-Plattformen (wie Arduino) ergibt sich die Möglichkeit, ein einfaches EMA-System aus sehr günstigen Komponenten zu entwickeln.

## **Aufgabenstellung**

Auf Basis von günstigen Sensoren und Mikrokontrollern, sowie freier open-source Software, soll ein preiswertes Messsystem zur Validierung von Simulationsmodellen entwickelt werden.

### **Arbeitspakete:**

- ▶ Festlegen der Anforderungen an das Messsystem
- ▶ Auswahl der Komponenten
- ▶ Entwicklung der Software zum Auslesen der Sensoren (Arduino)
- ▶ Evaluation der Auswertesoftware (open-source)
- ▶ Vergleich mit einem kommerziellen EMA-System
- ▶ Präsentation der Ergebnisse und Diskussion

**Aufteilung der Arbeit:** 70% Entwicklung/Programmierung, 20% Messen, 10% Bericht

**Anforderungen:** Erfahrung mit Programmierung; optimalerweise im Bereich Mikrocontroller (Arduino).

### **Kontakt:**

Nino Ceresa

PFA E 82

044 633 37 19

[ceresa@inspire.ethz.ch](mailto:ceresa@inspire.ethz.ch)



## **Acknowledgment**

I would like to thank Natanael Lanz for his aid in sensor characteristics, Daniel Spescha for his inputs on modal analysis and Nino Ceresa for his continued support while all was happening from remote locations during this unusual year.



# Contents

<b>1</b>	<b>Introduction</b>	<b>1</b>
1.1	Motivation . . . . .	1
1.2	Related Work . . . . .	1
1.3	Overview . . . . .	2
<b>2</b>	<b>State of the Art</b>	<b>3</b>
2.1	Measurement . . . . .	3
2.1.1	Measurement and Instrumentation . . . . .	3
2.2	Sensors and Transducers . . . . .	4
2.2.1	Sensor Types . . . . .	4
2.2.2	Transducer Principles . . . . .	6
2.3	Signal Conditioning and Processing . . . . .	10
2.4	Experimental Modal Analysis . . . . .	11
2.4.1	Frequency Response Measurement . . . . .	12
2.5	Electronic Components . . . . .	12
2.5.1	Passive Components . . . . .	12
2.5.2	Active Components . . . . .	13
2.6	Transmission Protocols . . . . .	14
2.6.1	Universal Asynchronous Receiver-Transmitter . . . . .	15
2.6.2	Serial Peripheral Interface . . . . .	16
<b>3</b>	<b>Signal Chain</b>	<b>17</b>
3.1	Amplification . . . . .	18
3.1.1	Operational Amplifier . . . . .	18
3.1.2	Mean Noise Figure and the Signal-to-Noise Ratio . . . . .	20
3.1.3	Instrumentation Amplifier . . . . .	23
3.2	Filtering . . . . .	24
3.2.1	Passive Lowpass Filters . . . . .	24
3.2.2	Optimizations of Lowpass Filters . . . . .	27
3.2.3	Active Filter Topologies . . . . .	35

3.2.4	Anti Aliasing Filter . . . . .	36
3.3	Analog to Digital Conversion . . . . .	37
3.3.1	Topologies . . . . .	38
<b>4</b>	<b>Data Acquisition and Software</b>	<b>39</b>
4.1	Data Acquisition . . . . .	39
4.1.1	Building Blocks . . . . .	40
4.1.2	Interfaces . . . . .	41
4.1.3	Dataflow . . . . .	42
4.2	Software . . . . .	43
4.2.1	Implementation . . . . .	43
4.2.2	Challenges . . . . .	44
<b>5</b>	<b>Test Setups</b>	<b>45</b>
5.1	System Costs . . . . .	45
5.2	Hammer-Hammer Test . . . . .	47
5.3	Andromeda Measurement . . . . .	47
5.4	Filter Test Setups . . . . .	48
<b>6</b>	<b>Results and Discussion</b>	<b>49</b>
6.1	Hammer-Hammer Test . . . . .	49
6.2	Andromeda Measurement . . . . .	49
6.3	Filter Test Setups . . . . .	52
<b>7</b>	<b>Conclusion and Future Work</b>	<b>53</b>
7.1	Conclusion . . . . .	53
7.2	Progress and Points of Transfer . . . . .	53
7.3	Future Work . . . . .	54
<b>A</b>	<b>Appendix</b>	<b>55</b>
<b>List of figures</b>		<b>59</b>
<b>List of tables</b>		<b>61</b>
<b>Bibliography</b>		<b>63</b>

# List of Abbreviations

<b>AAF</b>	Anti Aliasing Filter
<b>ADC</b>	Analog to Digital Converter
<b>ASCII</b>	American Standard Code For Information Interchange
<b>CMR</b>	Common-Mode Rejection
<b>CPU</b>	Central Processing Unit
<b>DAC</b>	Data Acquisition
<b>DC</b>	Direct Current
<b>EMA</b>	Experimental Modal Analysis
<b>FIFO</b>	First In, First Out
<b>FRF</b>	Frequency Response Function
<b>FT</b>	Fourier Transform
<b>MCU</b>	Microcontroller Unit
<b>MEMS</b>	Micro-Electro-Mechanical-Systems
<b>MISO</b>	Master In Slave Out
<b>MOSI</b>	Master Out Slave In
<b>MT</b>	Machine Tools
<b>LC</b>	Load Cell
<b>LPF</b>	Lowpass Filter
<b>LSB</b>	Least Significant Bit
<b>OPA</b>	Operational Amplifier
<b>I<sup>2</sup>C</b>	Inter-Integrated Circuit
<b>PCB</b>	Printed Circuit Board
<b>IC</b>	Integrated Circuit
<b>RS</b>	Recommended Standard
<b>SAR</b>	Successive-Approximation
<b>SCLK</b>	Serial Clock
<b>SNR</b>	Signal-To-Noise-Ratio
<b>SPI</b>	Serial Peripheral Interface
<b>SS</b>	Slave Select
<b>TF</b>	Transfer Function

**UART** Universal Asynchronous Receiver-Transmitter  
**USB** Universal Serial Bus

# 1

## Introduction

### 1.1 Motivation

The Experimental Modal Analysis (EMA) is a powerful tool for evaluating dynamic models of structures. Despite its extensive usage in the aerospace industry, in many other engineering fields the benefits of EMA are overshadowed by the initial investment and the operator costs of an EMA system. To enable Machine Tools (MT) manufacturers to test their products and validate their modal predictions. Progress in Micro-Electro-Mechanical-Systems (MEMS) technology enables the use of new generation of low-cost sensors in EMA.

### 1.2 Related Work

Considering the use of low-cost accelerometers in EMA specifically, a two-point vibration measurement system with a bandwidth of 500 Hz has been developed [3]. The authors Chan and Huang used this system to conduct a multiple-point vibration tests on a MT. Operating at lower frequencies, Beskyroun and Ma used MEMS based accelerometers to conduct an EMA on building structures. Because we aim for higher bandwidths in this thesis, the transmission protocols used in the previously mentioned works do not satisfy the required data transmission rates. Piana et al. developed a modal test system, which uses piezoelectric transducers that are typically used to tune musical instruments as response sensors [9]. Although giving an alternative option in the development of a low-cost system, this approach comes with two main drawbacks. Firstly, the sensors measure in one dimension only, compared to the now common three in accelerometer integrated circuits (ICs). Because of this, the system is unsuited for some use cases. Secondly, when using piezoelectric transducers, one needs to conduct dedicated signal conditioning for each sensor. In comparison, this is already integrated in accelerometer Integrated Circuit (IC)s that offer direct digital signal output. Hence more components must be used when going with the alternative option, increasing cost and form factor and decreasing reliability. Finally, a construction kit for a low-cost

### 1.3 Overview

vibration analysis system was proposed by Vollmer et al. back in 2009 [14]. According to this paper, a broad product line of capacitive accelerometer ICs, optimized for different bandwidths are available. But starting at a bandwidth of 2500 kHz and higher only accelerometer ICs with high acceleration ranges of  $\pm 70\text{ g}$  are available. For noise reduction, analog filters are sometimes partly or fully integrated. The noise in capacitive sensors can be expected to be in the range of 0.1...1 % of the measurement range, i.e. a factor of 100...1000 worse than in piezoelectric sensors.

In the field of civil engineering, bridges and skyscrapers require continuous vibration signal logging for structural health monitoring. This leads to an increased interest in driving down the cost of accelerometer based vibration monitoring systems. Girolami et al. has developed a low-cost MEMS systems for structural health monitoring of civil structures [5]. Typically, lower sensor bandwidths are required when analyzing building structures compared to MTs. The data rate of the proposed monitoring system does not suffice for this thesis.

Structural health monitoring is also required in rotary systems such as gas and wind turbines. Esu et al. integrated low-cost accelerometers in wind turbines and logged data via radio frequency to a central device [4]. An integration of digital accelerometer ICs with sampling rates of up to 1600 Hz has been tested under laboratory conditions.

Addressing low-cost impact hammer constructions, Waltham and Kotlicki implemented a piezoelectric transducer in a hammer, that is designed to trigger barbecue lighters [15]. The hammer was tested by impact against wooden planks. It yielded robust signal in a wide range of forces. In contrast to this work, the load cell used in this thesis is strain gauge base in order to be more cost-effective compared to the typical piezoelectric sensors used in impact hammers. For inexpensive calibration of a load cell used for modal testing, Wang et al. introduced practical techniques [16].

## 1.3 Overview

First fundamentals in measurement instrumentation, sensors and EMA is introduced in the state of the art. Then the Data Acquisition (DAC) developed for this project is presented in chapter 4. Testing environment are described in the chapter 5 and measurement results are discussed in results. Finally the conclusion gives reflects on the project.

# 2

## State of the Art

### 2.1 Measurement

The process of measurement is the comparison of data from the physical world in the frame of an agreed standard. It is carried out by using an instrument.

#### 2.1.1 Measurement and Instrumentation

Measurement instruments translate signals from the physical world into an agreed upon standard. These standardized signals can be compared, altered and stored. The original data acquired from the physical signal is usually in analog form. This is then converted to digital before it is passed on. The signal chain of a typical digital measurement instrument is shown in Figure 2.1. A detailed look at measurement instruments and its components is available in [17].

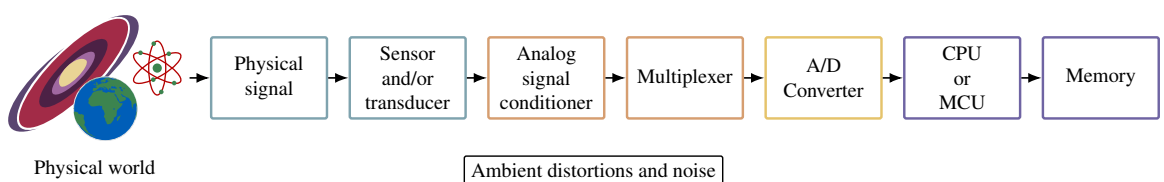


**Figure 2.1:** Digital measurement instrument

## 2.2 Sensors and Transducers

A device that responds to a changing phenomenon is called sensor. If we need to transfer from one energy from to another, we use a device called transducer. If one compares sensors and transducers based on the energy input and output, one identifies three types:

- In *modifiers* a specific energy form is not converted but modified. Hence they use the same form of energy as input and output.
- *Self-generators* give out electric signals from non-electric inputs without the need of additional energy.
- *Modulators* in contrast give out electric signals from non-electric inputs, but require an additional energy input.

As part of this we focus on self-generating piezoelectric sensors, capacitive modulators that convert mechanical deformation in a static electric field into an electric current, as well as strain gauge based modulators.

### 2.2.1 Sensor Types

Here we separate different sensors depending on physical value they respond to. In EMA we use a force input signal and measure a acceleration, velocity or displacement output signal. Where force is generally detected using Load Cells (LCs), the output signal is commonly detected by accelerometers at predefined point on the MT. But other setups may be used. Optical methods, for example, allow the detection of the output signal in a non-contacting manner and are preferred when testing very small structures. But for this thesis an approach with low-cost accelerometers is chosen. Therefore, a brief introduction to load cells and accelerometers is given. More on sensor types can be found in [17].

#### Load Cells

A force measurement sensor that converts a force into an electrical signal is called Load Cell (LC). The basis of force measurement results from the physical behavior of a body under external forces. Depending on the bandwidth and magnitude of the signal, as well as the duration of the signal capture, different methods of force measurement are applied in various designs. The methods in brief are [17]:

- Balancing the unknown force against a standard mass through a system of levers
- Measuring the acceleration of a known mass
- Equalizing it to a magnetic force generated by the interaction of a current-carrying coil and a magnet
- Distributing the force on a specific area and then measuring the pressure
- Converting the applied force into the deformation of an elastic element

Furthermore, these methods can be combined with different designs of measuring equipment. Each of which addressing two main problems. First, the physical and geometrical constrains by the application of the device and second, the means by which the force can be converted into an electrical signal.

## Accelerometers

Accelerometers are sensors that convert acceleration into an electrical signal. In order to measure a physical phenomenon we use seismic masses that act on the sensor structure based on their inertia properties. For example, it is the structure in strain gauge based accelerometers that translates the inertia force into a deformation, where capacitive sensor structures may use deformations or relative motions of separate components in an electric field. In piezoelectric accelerometers the seismic mass deforms a piezoelectric material, see Figure 2.2. This is the simplest setup of so called seismic accelerometers.

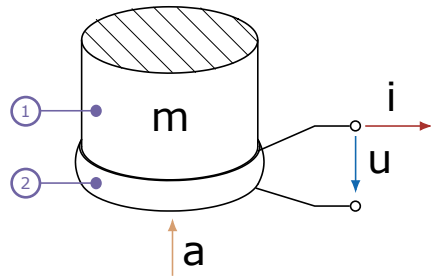


**Figure 2.2:** Function principle of a piezoelectric accelerometer

---

a	: Acceleration
m	: Mass
i	: Induced Current
v	: Induced voltage
(1)	: Seismic mass
(2)	: Piezoelectric material

---

**Table 2.1:** Legend to Figure 2.2

In seismic accelerometers the base of the arrangement is motion. When describing the one dimensional case, one can express non-stationary random vibrations acting on the accelerometer as

$$m \frac{d^2 z}{dt^2} = c \frac{dz}{dt} + kz = mg \cos(\theta) - m \frac{d^2 x_1}{dt^2} \quad (2.1)$$

where

- $m$  is the seismic mass
- $z = x_2 - x_1$  is the relative motion between the mass and the base
- $x_1$  is the displacement of the base
- $x_2$  is the displacement of the mass
- $\theta$  is the angle between sense axis and gravity

The Laplace transformed second-order system thus takes the form

$$G(s) = \frac{X(s)}{F(s)} = \frac{K}{s^2/\omega_n^2 + 2\zeta s/\omega_n + 1} \quad (2.2)$$

where

- $s$  is the Laplace operator
- $K = 1/k$  is the static sensitivity
- $\omega_n = \sqrt{k/m}$  is the undamped frequency in rad/s
- $\zeta = c/2\sqrt{km}$  is the damping ratio

It is obvious that the performance of accelerometers depends on their static sensitivity, the natural frequency and the damping ratio. We want the accelerometer to have a linear transfer function in the range

## 2.2 Sensors and Transducers

of operation. But namely the damping ratio can distort a measurement when operating an accelerometer near its eigenfrequency, see Figure 2.3. This is the most simplified case, that measures the acceleration in one dimension. In three dimensional accelerometers, that are generally used in EMA, the acceleration becomes a function of  $d^2x/dt^2$ ,  $d^2y/dt^2$  and  $d^2z/dt^2$ . Consequently, multiple transducers in multiple channels are used.

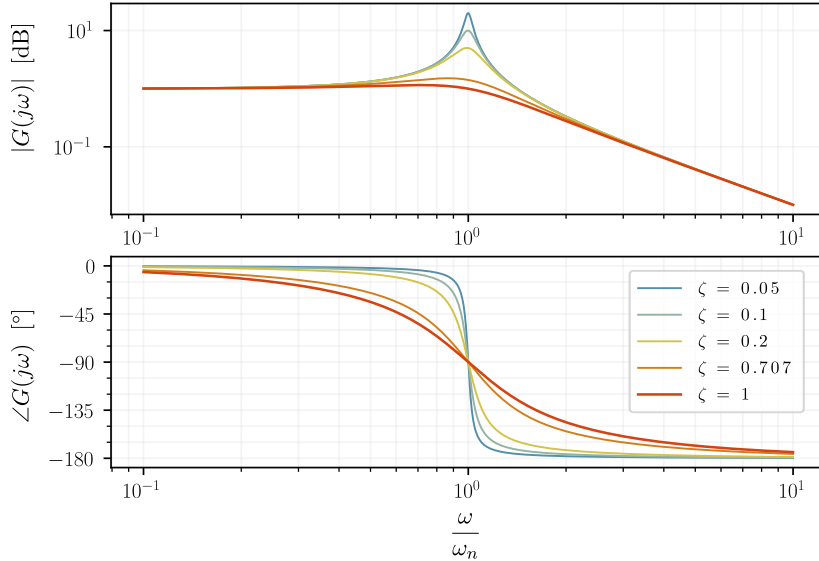


**Figure 2.3:** Bode plots of second order system describing the dynamic behavior of seismic accelerometers

### 2.2.2 Transducer Principles

The same transducer types can be used in LCs and accelerometers due direct relation between acceleration and force in inertial models. Namely in commercially available EMAs, piezoelectric transducers are typically used in both the LCs and accelerometers. In this section the physical principles of transducers used in this thesis are presented.

#### Strain Gauges

In strain gauge LCs and accelerometers the elastic properties of a material probe is exploited.

Given a probe, we apply a controlled load through an external force in LCs or through the seismic mass in accelerometers. This load deforms the probe in the elastic region and the deformations are captured by a strain gauge at a suitable location. The probe deformation is proportional to the force acting on the probe because of Hooke's law.

The strain gauges themselves each use a specific length gauge wire in order to reach a resistance of typically  $120 \Omega$ . The wire is bonded between two thin sheets in coiled up form as can be seen in Figure 2.4a. The sheets act as insulating carrier and can be easily deformed with the intent of passing the load to the wire grid. The gauge is attached to the probe structure by a wax or a resin. The intent is that deformations in transversal direction of the strain gauge act on all coils simultaneously, changing their resistance. By using small sized strain gauges with respect to the probe, the mechanical and thermal properties of the strain

gauge become negligible small. As an example, we assume the probe expands. Then a strain gauge on its surface experiences tension. The coils in the grid are therefore stretched and as a result of the generalized Hook's law the coil cross sections decrease. Both the strain in axial direction of the coil and the decreased coil cross sections increase the wire's resistance.

In order to measure deformations one needs to take environmental influences into consideration. It is well known that resistance is susceptible to variations in temperature. Placing the strain gauge in a wheatstone bridge, with resistors, that change their resistance in the same manner as the strain gauge will reduce the influence of temperature significantly, see Figure 2.4b.

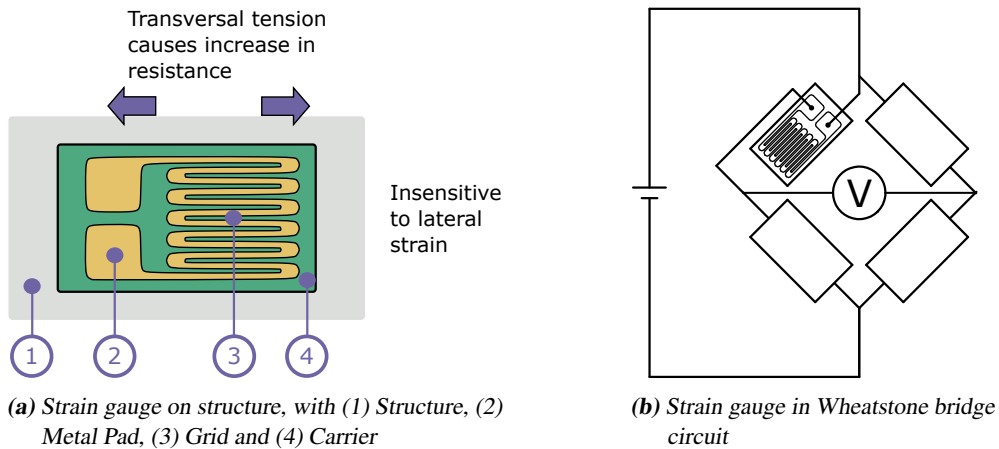


**Figure 2.4:** Strain gauge

## Piezoelectric Materials

Some materials develop electric charge proportional to directly applied mechanical stress. The same materials show the converse effect. A proportional strain of the material will occur to an applied electric field.

The first phenomenon has found its application in a variety of self-generating sensors that output electrical signals, namely in LCs and accelerometers, where the piezoelectric charge is converted into a current or voltage signal.

Piezoelectric sensors are designed to exploit the piezoelectric effect of the material in one axis. Additionally, we use amplifier circuits so that the weak electrical signal, induced due to the piezoelectric charge, is elevated to amplitudes that are in the range of operation of standard electronic components. These circuits require additional energy. Commercially available LCs therefore require supplied energy, see Figure 2.5.

Depending on the design of the sensor, piezoelectric materials are used in different shapes. Figure A.1 shows some possible variations.

## Capacitive Transducers

In capacitive transducers the electric field of a capacitor is used as reference. Changes in the electric field of a sensing capacitor generate an electrical signal output at the surrounding circuit. That is, if we change the supply voltage or capacitance of said capacitor, the signal output is non-zero. This gives a broad framework of different transducers that normally use charge-discharge or constant input signals,

## 2.2 Sensors and Transducers

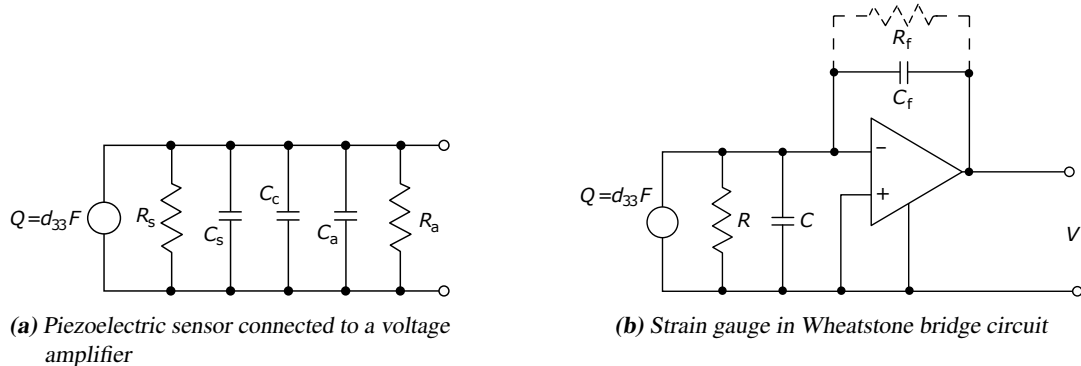


**Figure 2.5:** Piezoelectric sensors connected to amplifier circuits [17]

which enable us to measure either the capacitance or the change in capacitance. The simplest capacitor design consists of two parallel electrodes with capacitance  $C$ .

$$C = f(d, A, \varepsilon) \quad (2.3)$$

With variable distance, dielectric material or area and with the measurement of the capacitance, we can then deduce the plate displacement in normal and parallel direction to the plates depending on the method used, see Figure 2.6. In the following we present some models of the capacitance derived from the chapter written by Eren [17].

In *variable displacement* transducers, the distance between two capacitive plates is inversely proportional to the capacitance.

$$C(x) = \frac{\varepsilon A}{x} = \frac{\varepsilon_r \varepsilon_0 A}{x} \quad (2.4)$$

where

- $\varepsilon$  is dielectric constant or permittivity
- $\varepsilon_r$  is the relative dielectric constant (in air and vacuum  $\varepsilon_r \approx 1$ )
- $\varepsilon_0$  is  $8.854\ 188\ \text{F/m}$ , the dielectric constant of vacuum
- $x$  is the distance of the plates in m
- $A$  is the effective area of the plates in  $\text{m}^2$

In *variable area displacement* transducers, the capacitance is proportional to the reduction of area due to the movement of the plate.

$$C(x) = \frac{\varepsilon_r \varepsilon_0 (A - wx)}{d} \quad (2.5)$$

where

- $\varepsilon_2$  is the permittivity of the displacing material (e.g. liquid)
- $w$  is the width
- $wx$  is the reduction in the area due to movement of the plate
- $d$  is the distance of the plates in m

In *variable dielectric* transducers, the capacitance depends on the ratio of each permittivity in the electric field.

$$C(x) = \epsilon_0 w [\epsilon_2 l - (\epsilon_2 - \epsilon_1)x] \quad (2.6)$$

where

- $x$  is the displacement normal to the plate's direction
- $\epsilon_1$  is the relative permittivity of the dielectric material
- $\epsilon_2$  is the permittivity of the displacing material (e.g. liquid)

*Differential displacement* sensors are setup in capacitive arrangements that aim to eliminate nonlinearities. Different variations of these types of sensors exist. For example we can allow the outer plates to move and fix the middle one or we can reverse this setup. But the range is equal to twice the separation in both cases.

$$\begin{aligned} 2\delta C &= C_1 - C_2 = \frac{\epsilon_r \epsilon_0 lw}{d - \delta d} - \frac{\epsilon_r \epsilon_0 lw}{d + \delta d} = \frac{2\epsilon_r \epsilon_0 lwd}{d^2 + \delta d^2} \\ C_1 + C_2 &= \frac{\epsilon_r \epsilon_0 lw}{d - \delta d} + \frac{\epsilon_r \epsilon_0 lw}{d + \delta d} = \frac{2\epsilon_r \epsilon_0 lwd}{d^2 + \delta d^2} \end{aligned}$$

Giving approximately

$$\frac{\delta C}{C} = \frac{\delta d}{d} \quad (2.7)$$

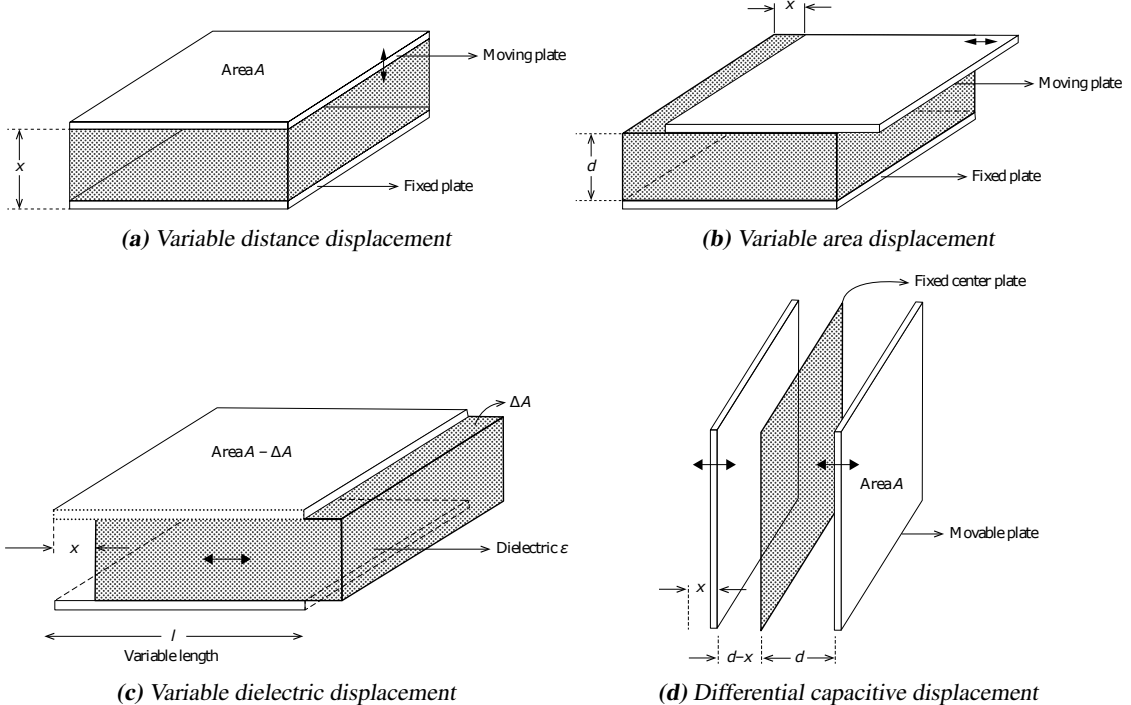


**Figure 2.6:** Capacitive displacement transducers [17]

## 2.3 Signal Conditioning and Processing

Given a sensor design, one can then map the displacement of the respective transducer to the load acting on a LC, respectively, when using a seismic mass and the corresponding equation of motion, to the acceleration measured by an accelerometer. The capacitive displacement transducer is applicable for many sensor applications and the fact, that the sensing conductors can be built from a variety of materials and can be optimized for different input voltage levels, makes its form factor scalable in both directions. In a sensor IC package, the capacitive transducers can be realized in a smaller form factor or with higher precision at the same size compared to resistive sensors, like strain gauges. A simplified model of the mechanics inside a capacitive MEMS sensor are shown in Figure 2.7.

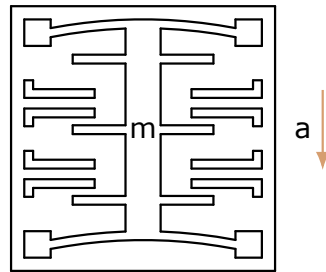


**Figure 2.7:** Capacitive MEMS accelerometer, with acceleration  $a$  and the seismic mass  $m$ . The bridges attached to the seismic mass act as dielectricum.

## 2.3 Signal Conditioning and Processing

In an ideal world, the signal output of a sensor would correlate to the measurand exactly. In real systems this is not the case because of a variety of reasons. In low-frequency applications, the most important ones are:

- The voltage or current rating at a sensor's output is not perfectly linear with respect to the measurand. Often the output is pseudo-linear in a limited range of values and deviates from the trajectory for values outside of this range.
- Noise and shifts introduced through the inherent impedances of analog components lead to deviations from the voltage or current rating of the sensor as well as deviations of these ratings with respect to the measurand itself.
- The quantization process causes the captured value space to have a finite resolution.
- Analog signals can only be digitized with a finite sampling rate. A discrete set of data points is captured instead of a continuous signal.

The field of signal processing includes analyzing, modifying and synthesizing signals. Most prominently, in data acquisition systems we convert analog signals to digital ones that can be further processed without the parasitic effects of the analog realm. On the opposite side when addressing these parasitic effects one needs to apply signal conditioning. In other words, before every processing step of an analog signal we need to consider signal conditioning. When dealing with digital signals, no signal conditioning is required.

## 2.4 Experimental Modal Analysis

EMA is a powerful tool to detect vibration related problems of mechanical structures. We use modes to characterize resonant vibrations of the system. This section is only a short excerpt of an introduction to EMA. An overview has been presented by Schwarz and Richardson in [10].

### Vibration

In every vibration one can observe a combination of two different types of vibrations. The forced and the resonant ones. Forced vibrations in a structure are caused by

- Internally generated forces
- Unbalances
- External loads
- Ambient excitations

Common examples of vibration sources in MT are displayed in Figure 2.8.

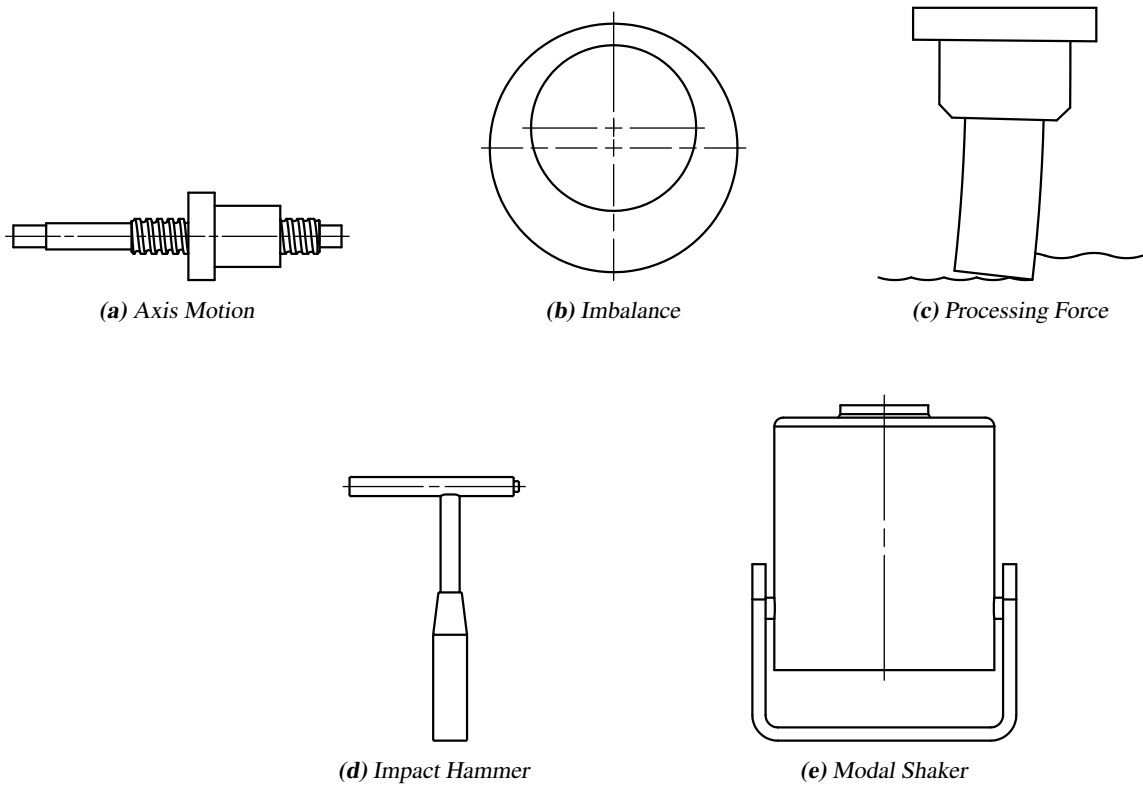


**Figure 2.8:** Sources of forced vibration. Note that (a), (b) and (c) occur during MT operation, while (d) and (e) are devices that are explicitly used for EMA to introduce vibrations into the structure of investigation.

Resonant vibration arises when one or more of the natural modes of vibration, inherent properties of the structure under investigation, is excited. Resonant vibration typically amplifies the vibration response to a level that exceeds deflection, stress and strain caused by static loading.

### 2.4.1 Frequency Response Measurement

In an EMA one needs to determine the Frequency Response Function (FRF) from input to output. To achieve this we measure the so called response or output function of the structure under investigation. The measurement instrument for this task uses a signal chain in form of 2.9.

- The sensor on the structure translates the physical value (acceleration, velocity or position) into an electrical voltage or current, the analog signal variable.
- The amplifier amplifies the typically low power signal to fit it to the input range of the Analog to Digital Converter (ADC).
- The ADC samples and quantizes the analog signal. It is then converted into a digital signal, in which the quantity is expressed in form of a binary code.
- The discrete time signal is then stored on the computer memory.

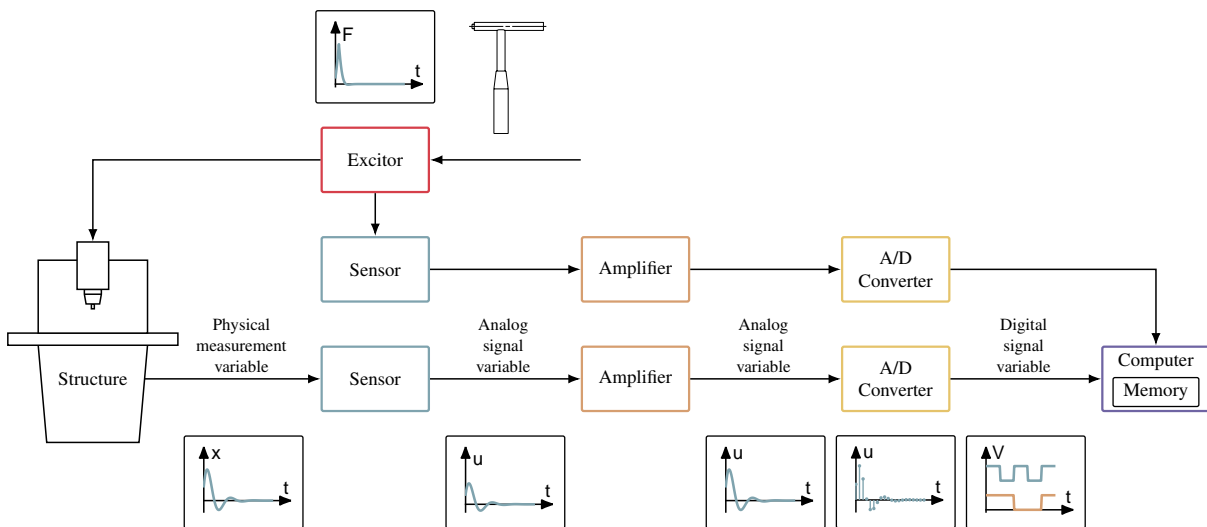


**Figure 2.9:** FRF measurement setup

## 2.5 Electronic Components

This section serves as an introduction to the function of selected electronic components and circuits. It does not give a complete overview of the state of the art. For more background on electronics [12] and [13] may be consulted.

Electronic components are divided into two main types; passive and active ones. Where active components are allowed to generate, amplify or oscillate an electrical signal, passive components can only absorb, dissipate or store electric energy.

### 2.5.1 Passive Components

Because of the increase in digital processing, the number of passive components has decreased drastically in modern electronic circuits. This, in addition to the trend of using more complex devices in favour to

multiple simple passive components, has led to a great variety of passive components which are designed with emphasis on reliability.

Typical examples of passive components are:

- *Wires* Depending on the mechanical requirements for the wire, it can either be designed with a solid core or a stranded wire core. A wire consisting of multiple smaller diameter conductors shows better flexibility but reduced current-carrying capacity at the same wire diameter. This is because of the smaller overall conductor cross-section of a stranded wire and, when transmitting high frequency signals, a greater power dissipation due to the more prevalent skin effect. Furthermore the simplicity of solid core wires makes them more resistant to corrosion and more suitable to be used in harsh environments.
- *Resistors* Depending on the application different types of resistors can be applied. Fixed value resistors, can be used for safety of other components by dissipating heat or reducing to set the current and voltage in combination relative to other devices. Variable resistors change their value due to different physical phenomena. Thermistors show resistances that are highly susceptible to temperature changes, potentiometers resistance is manually tunable and photoresistors show a light dependant resistance, to name a few.
- *Capacitors* store energy in form of an electric field. They have many applications, most prominently in filter circuits and as bypass capacitors to reduce smooth out non constant power draws.
- *Inductive Devices* Are devices that store energy in form of an electric field. In modern devices coils are less common due to benefits, when realizing the circuit with capacitors instead. But in specialized applications, namely when converting between electrical and mechanical signals, i.e. in motors, generators, loudspeakers etc.
- *Transformers* transfer electrical energy from circuit to circuit. Step-up transformers increase the voltage of high alternating current, where step-down decrease the voltages in exchange for higher currents.

### 2.5.2 Active Components

Active components enable the control of high energy signals using small input signals. If the control happens to be continuous and proportional to the input signal, the component used is called linear amplifier. Because of their function, active components typically require additional power supply. Most components of this type include doped semiconductors, therefore conservatively passive semiconductor component are categorized in the group of active components as well. Finally, power sources that don not control signals based on small inputs but rather convert other forms of energies into electrical ones, are included in active components too.

- *Diodes* are non-linear components with an asymmetrical current-voltage curve. Because of this the diode is directional where, conventionally defined current is only allowed to flow from anode to cathode. Its analogous in a water circuit is a check valve.
- *Bipolar transistors* can be used as amplifier or trigger and are based on semiconductors that are doped with both carriers, i.e. electrons and holes. Depending on the surrounding one can amplify voltages, currents or powers with bipolar transistors, but the transistor itself is current controlled.
- *Field transistors* or uni polar transistor is doped using only one of the two types of carriers compared to the bipolar transistor. They are voltage controlled.

## 2.6 Transmission Protocols

- In an *Integrated Circuit (IC)* a complete circuitry is produced on a carrier material. Multiple consecutive steps of diffusion, oxidation and etching of a semiconductor result in a multi-layered structure. ICs come in packages that are a fraction of the size a circuit of classical components would use. For the categorization of those packages one can look at Figure A.2. The use of ICs increases reliability and maintainability and decreases costs, whenever it is possible to replace a conventional circuit.
- The *Operational Amplifier (OPA)* is a multi-stage, high gain and galvanically coupled differential amplifier. Consisting of multiple transistors in an IC, the properties of OPAs surpass the ones of single transistors in many designs. Namely, higher gains are possible due to the reduction of the amplified noise.

## 2.6 Transmission Protocols

Digital transmission protocols offer established standards for the communication between ICs and devices that at least include a processing unit. There exists a plethora of protocols, that address the communication on a range of different levels of abstraction. Theoretically, these levels can be categorized according to the Operational Amplifier model (OPA model), but it is obvious that most protocols address issues on multiple levels. Nevertheless, the model is useful when establishing a new network, since all steps, necessary for a successful communication, are best traced in order of the model. The OPA model includes seven layers, as seen in Figure 2.10.

1. The *physical layer* defines the physical form of the data transmission, i.e. the medium, in which the data is transmitted and the physical connections.
2. The *data link layer* addresses the transmission conditions and standards, which allow the communication between two or more devices.
3. In the *network layer* we implement the definitions for the shortest connections, error detection and addressing techniques.
4. The *transport layer* ensures that all data is transparent and securely transmitted. Its segmented data is used to detect duplicates and missing data.
5. The *session layer* establishes channels between devices. It manages open connections and synchronization.
6. It is the *presentation layer*, where one defines the syntax and semantics of the code.
7. And the *application layer* that provides the protocols and services that are used in applications. This is the data directly available to the end-user.

When dealing with real hardware, the level of abstraction that can be reached will be limited depending on the device. Namely in the communication between Microcontroller Unit (MCU)s the different low end communication protocols can be used to communicate between ICs. Many smart devices of today use the Inter-Integrated Circuit ( $I^2C$ ), the Serial Peripheral Interface (SPI) or both connections to access their registers. With these protocols two respectively, four wires connect two devices over short distances. When the distance increases or the environment gets noisy, one needs to improve the cable's isolation, insert active signal repeaters, or switch to another transmission standard. The transmission standard RS-485, defines a widely adopted industry standard of differential digital signal transmission. These offer more stable signal transmissions in harsh environments and over long distances with the caveat of using

two wires for each signal. In depth information about data communication protocols is available in the handbook [2] Rs intro [8]

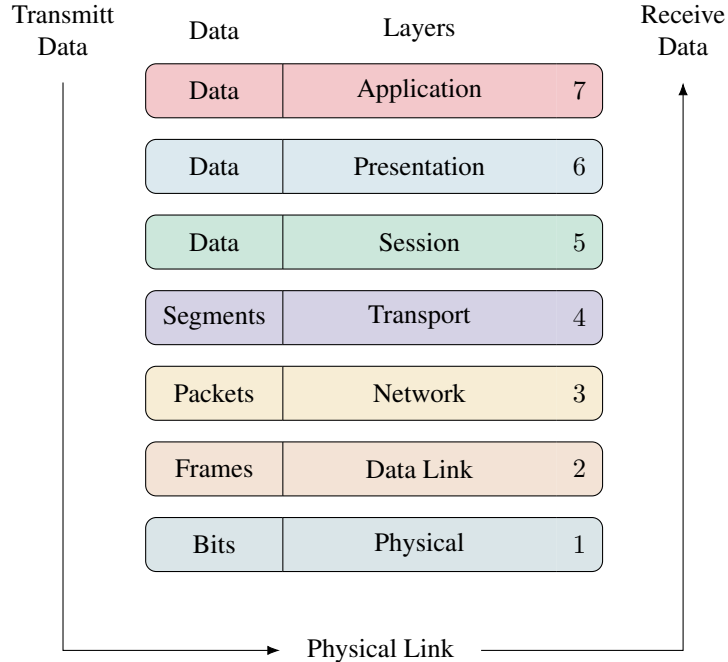


**Figure 2.10: OSI Model**

### 2.6.1 Universal Asynchronous Receiver-Transmitter

The Universal Asynchronous Receiver-Transmitter (UART) protocol is a widely adopted, low-level interface that does not specify the data format or speed. The receiver and transmitter are connected by one wire, that transfers serial bits in form of two voltage-levels, high and low. Both devices must be configured to the bit rate for successful signal transmissions. Where the bit rate defines the number of physically transferred bits per second:

$$R_b = \frac{1}{T_b} \quad (2.8)$$

Which is correlated to the baud rate, which defines the transferred symbols in bauds per second (Bd/s):

$$f_{\text{sym}} = \frac{R}{N} \quad (2.9)$$

where the information per pulse  $N$  defines the number of bits per pulsed bit. Note that digital systems that use binary code  $N = 1$  and therefore  $f_{\text{sym}} = R_b$ . We often use a two-wire setup of UART to enable full-duplex transmission between two devices.

### RS-458

RS-458, or EIA-485 is a standard that defines the driver characteristics of a differential serial communication system that has found a wide adoption in industrial control systems. It defines the characteristics of

## 2.6 Transmission Protocols

the transmitter and receiver on the physical layer only. Therefore, it does not specify the communication protocol and any serial transmission protocol may be transmitted via this connection. Because it is differential, it uses two channels, labeled A and B, to transmit one signal at a time. In a transmitter the input serial signal is converted two signals of reversed magnitudes. The receiver then reconstructs the original signal by using the difference between the two signals. This is much more reliable than single wire signal, since it can be assumed that all environmental disturbances act on both channels equally, introducing no change to the differential signal between the two. The additional connector C, specified defines the drivers ground.

### 2.6.2 Serial Peripheral Interface

The SPI interface defines a serial connection between two or more devices that requires at least three wires. All transmissions are initiated by a master device, that sends registry addresses as requests. Slave devices, if active, send the data from the requested registry on to the Master In Slave Out (MISO) wire. The Serial Clock (SCLK) is carrying the master clock, defining the baud rate for all signal transmissions. The Slave Select (SS) pin activates the slave transmission. A slave can only send and receive if the SS pin is activated, which usually means that it is low. This pin can be ignored if only one slave device is present. Because of the naming convention of the data wires, the pins with the same names are connected if one links the master with a slave device. That is MISO to MISO and Master Out Slave In (MOSI) to MOSI. When daisy chaining multiple slave devices one needs to link the wires with reverse naming, to ensure data transmission in series. In this mode all slave devices are active at the same time and each appends its registry data to the previous ones. The typical bus setups can be seen in Figure 2.11.

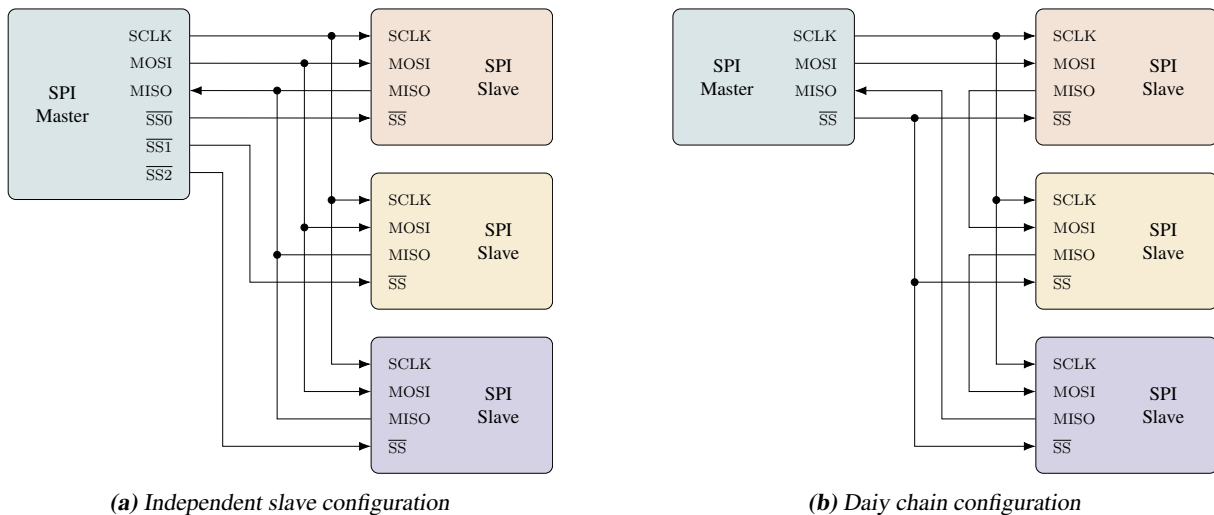


**Figure 2.11:** SPI bus configurations

# 3

## Signal Chain

Some sensors operate at small energies. The signals are too weak to be converted into digital ones by standard components. *Signal conditioning* enables us to amplify and denoise analog signals so that the signal can be further processed. In our application, both the load cell's and accelerometer's sensors signal must be amplified to match the input range of their respective ADC. In this section we put together all conditioning steps necessary from sensor to the digital signal under the term signal chain. Because the selected accelerometers come in IC packages that include the complete signal chain, we focus on the signal chain of the load cell. For a quick introduction into signal conditioning and processing, read Section 2.3. A schematic of a typical signal chain of an EMA is shown in Figure 2.9.

LCs that are based on strain gauges or piezoelectric ceramics both generate low-voltage respectively low-current signals when under stress. In strain gauge LCs, it is the resistance that changes when it is stressed. Therefore, an electric energy supply is necessary to be able to generate a sensor signal. This makes the sensor an active one. With piezoceramics, it is possible to measure the current induced solely by the piezoelectric effect, which makes it passive; but especially in small sensors, preconditioning circuits are already integrated in the sensor so that one needs additional supply voltage for the conditioning and to get an amplified current or voltage signal. When looking at the voltage output signals, they vary in the range of a few mV. Standard components operate in the range of a few volts; therefore we need to amplify the signals first, if we want to use low-cost conditioning. The key components used to condition analog signals are filters. They are used to reduce the bandwidth to the range expected to be measured, cutting off unnecessary noise from outside this bandwidth. The last processing step in the analog signal chain is the conversion of the signal into a digital one, that is from a time-continuous, continuously valued signal into a discrete time-step and quantized one. This conversion presupposes the signal to be conditioned, so that the value range and frequency bandwidth are both limited to the maximum operation range of the ADC, to meet the best possible resolution in time and amplitude of the signal in the digital realm. This can be achieved using at least one amplifier and one Lowpass Filter (LPF).

## 3.1 Amplification

The power of electrical signals is amplified by active electrical components that are configured to match different properties.

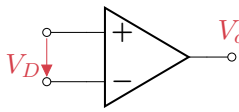
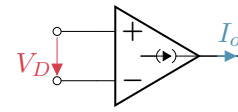
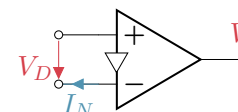
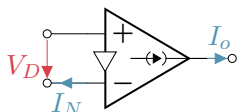
- The *gain* of an amplifier is a measure of the relative signal amplitude between output and input. Amplifiers with higher gains require smaller input signals for the same output amplitudes and are therefore more sensitive.
- The *bandwidth* is the frequency range of satisfactory performance of an amplifier. Typically non-linear effects outside this region disturb the output signal.
- *Efficiency* defines how much of the supply power can be converted into the output signal. Depending on the technology used, the efficiency may vary between 10 and more than 90 %. Note that lower efficiency amplifiers generate more heat during operation.
- *Linearity* is a measure of how consistent the amplifier approaches a constant gain within its bandwidth. Typically, negative feedback loops are used to reduce non-linearities.
- *Noise*, a side effect generated by all electronic components, is given by the noise factor, that is a comparison between the output signal noise and the thermal noise of the input signal.
- The *output dynamic range* defines the ratio between the maximally allowed output signal power and the noise level of the system.

### 3.1.1 Operational Amplifier

Amplifiers apply signal gain on electrical inputs so that the output matches the input times a constant gain factor. The latter is determined by the impedance of the subsequent device in the signal chain and the magnitude at the input. But by setting the gain factor one predetermines the introduced absolute noise due to the amplifier's Signal-To-Noise-Ratio (SNR).

In simple amplifiers, the SNR purely depends on the quality of the components and the environmental conditions. This can be bypassed by building differential setups, where amplifiers, like transistors and field transistors, are fed with both the non-inverted and the inverted input signal individually. With multi-staging and additional filter circuits one can reduce the noise further and ultimately the SNR becomes strongly dependent on the circuit design and less dependent on the quality of each component. Specific to different applications, many variants of the described circuitry are available in so-called Operational Amplifiers (OPAs).

OPAs are available in a variety of IC packages and differ little from discrete transistors in terms of size and price. In some packages even multiple individual OPAs are included. Initially OPAs offered high accuracy at low frequencies. Over time different circuit designs for different needs have broadened the field of application considerably. Today, it is hard to find a task that is better met by a transistor than by an OPA. We subdivide the latter into four main types, as shown in Figure 3.1. The differences are high-resistive or low-resistive inputs and outputs. The standard OPA and the transconductance amplifier, for example, have high-resistance inputs. Therefore, they are voltage controlled. The outputs on the other hand are of low and high internal resistance respectively, where low-resistance outputs act as voltage sources and high-resistance outputs act as current sources. In the naming convention the two leading letters represent input and output. "V" at first position stands for a voltage controlled OPA with a high-resistance input, where "C" means current controlled and low-resistive input. At the second position "V" and "C" define

	Voltage output	Current output
Voltage input	Standard OPA VV-OPA  $V_o = A_D V_D$	Transconductance amplifier VC-OPA  $I_o = g_{m,D} V_D$
Current input	Transimpedance amplifier CV-OPA  $V_o = I_N Z = A_D V_D$	Current amplifier CC-OPA  $I_o = k_I I_N = g_{m,D} V_D$

**Figure 3.1:** Main operational amplifier types [13]

low- and high-resistance outputs that act as voltage and current source respectively. The differential gain of an ideal VV-OPA is given by the slope at the operating or bias point:

$$A_D = \left. \frac{dV_o}{dV_D} \right|_b \quad (3.1)$$

The transfer characteristics of an ideal OPAs can be seen in Figure 3.2. When dealing with current outputs the differential transconductance  $g_{m,D}$  indicates the degree of output current increase with rising input voltage.

$$g_{m,D} = \left. \frac{dI_o}{dV_D} \right|_b \quad (3.2)$$

Although the major part of electronics is based on voltage controlled circuits, OPA designs, different from the standard OPA are preferable in some applications. Amplifiers with low-resistance inputs are better suited for high frequency applications. The main advantages of the latter are the lower oscillation tendency due to shortened internal signal paths and larger range of possible gains compared to high-resistance input OPAs. When designing circuits with current amplifiers it is often easier to use the current transfer factor  $k_I$  than the differential transconductance.

$$k_I = \left. \frac{dI_o}{dI_N} \right|_b \quad (3.3)$$

Because of the differential circuit of the standard OPA, it is normally powered by a symmetric voltage supply. But when working with digital circuits, one usually uses single power supplies. For these applications OPAs were designed, that allow single supply voltage operation. Furthermore when one cannot use a higher voltage power supplies, rail-to-rail OPAs will allow control of the signal output between the full range of the positive and negative supply voltage, allowing maximal amplification, see Figure 3.3. When working with digital circuits, a single voltage supply is preferred. For this case one uses single supply voltage OPAs. In this thesis OPAs that were able to use both single and dual supply voltages were used.

### 3.1 Amplification

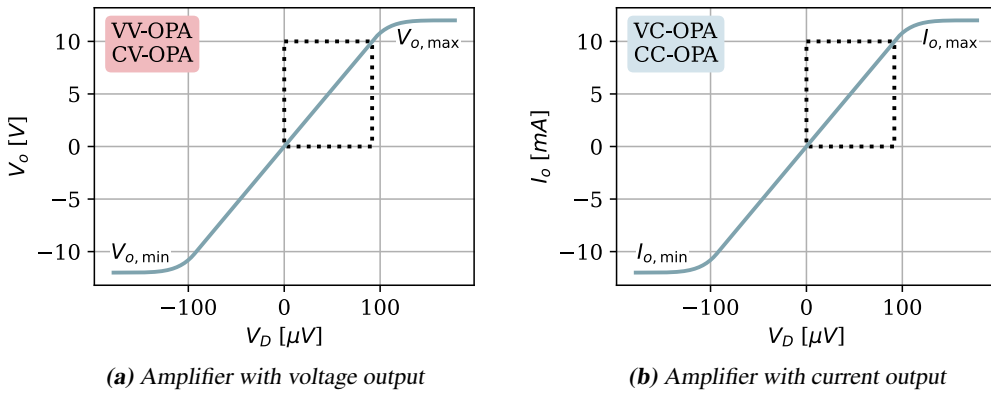


**Figure 3.2:** Transfer characteristics of OPAs, where the dotted square includes the line of positive operating or bias points.

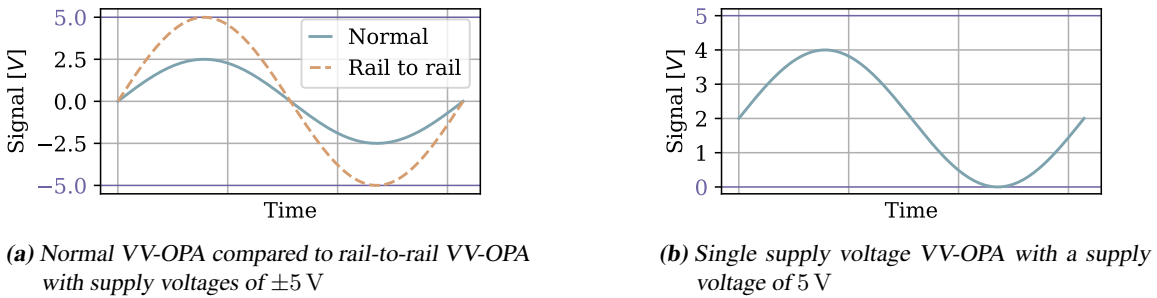


**Figure 3.3:** Controllability of VV-OPA signal outputs

#### 3.1.2 Mean Noise Figure and the Signal-to-Noise Ratio

To determine the mean noise figure and the Signal-To-Noise-Ratio (SNR) one needs conduct tests on an amplifier with a known signal. In its simplest form one can determine the SNR and the mean noise figure by connecting a signal generator directly to the amplifier's input. In [13] Tietze write, that per definition, the SNR is the ratio of the information containing signal power over the noise power:

$$\text{SNR} = \frac{P_{us}}{P_n} \quad (3.4)$$

where  $P_n$  is the power in the application specific frequency interval  $f_L < f < f_U$ . We know that the power is proportional to the square of its effective value. The effective value, on the other hand, is defined as the root-mean-square of the electrical signal. Hence the noise of the signal generator is:

$$\text{SNR}_g = \frac{\nu_{g,\text{eff}}^2}{\nu_{r,\text{eff}}} = \frac{\nu_{g,\text{eff}}^2}{\int_{f_L}^{f_U} |\nu_{r,g}(f)|^2 df} \quad (3.5)$$

An amplifier increases the noise density by the *spectral noise figure*  $F(f)$ . The SNR at the amplifier input is thus:

$$\text{SNR}_i = \frac{\nu_{g,\text{eff}}^2}{\nu_r} = \frac{\nu_{g,\text{eff}}^2}{\int_{f_L}^{f_U} |\nu_r(f)|^2 df} = \frac{\nu_{g,\text{eff}}^2}{\int_{f_L}^{f_U} F(f) |\nu_{r,\text{eff}}(f)|^2 df} \quad (3.6)$$

which is lower than the SNR of the signal generator. Note that in a circuit, it is the comparison between the powers of the useful signal and the input noise, that determines the quality of the signal that is amplified. If the input signal is too low compared to the input signal noise, the noise contribution will dominate in the amplified signal.

The *mean noise figure* corresponds to the relation of the SNR ratios:

$$F = \frac{\text{SNR}_g}{\text{SNR}_i} = \frac{\int_{f_L}^{f_U} F(f) |\nu_{r,g}(f)|^2 df}{\int_{f_L}^{f_U} |\nu_{r,g}(f)|^2 df} \quad (3.7)$$

And is usually quoted in decibels dB

$$F_{\text{dB}} = 10 \log F \quad F_{\text{dB}} = \text{SNR}_{g,\text{dB}} - \text{SNR}_{i,\text{dB}} \quad (3.8)$$

When using an ideal signal generator, that has uniform noise density over all frequencies, (3.7) simplifies to:

$$F = \frac{1}{f_U - f_L} \int_{f_L}^{f_U} F(f) df \quad (3.9)$$

Additionally, one can often assume the noise figure to be constant. Thus  $F = F(f)$ , which is generally referred to as the noise figure  $F$ .

In some applications the noise causes stronger interference in certain ranges of the given frequency interval than in other ranges. Then a weighted filter, whose absolute frequency response is proportional to the disturbing effect, is used to get more meaningful SNRs. For this the noise density of the generator in the denominators of Equations 3.5 and 3.6 are replaced by the *weighted noise density*:

$$|\nu_{r(B),g}(f)|^2 = \left| \vec{H}_B(2j\pi f) \right|^2 |\nu_{r,g}(f)|^2 \quad (3.10)$$

with the transfer function of the weighted filter  $\vec{H}_B(s)$ .

Note that the bandwidth of the amplifier needs to cover at least the interval of the useful signal  $f_L < f < f_U$  to provide equal amplification. Moreover, the bandwidth of the amplifier is usually wider than required, i.e. it amplifies the ranges  $f < f_L$  and  $f > f_U$  with operating gain  $\mathbf{A}_B(s)$ . It is in these ranges, where the signal only contains noise. Which means, that the amplifier, if not limited to the frequency range, provides the noise power at the output:

$$P_{n,o} = \int_0^\infty |\mathbf{A}_B(2j\pi f)|^2 F(f) |\nu_{r,g}(f)|^2 df \quad (3.11)$$

Considering that the signal is amplified by the useful gain  $\mathbf{A}_{B,us}$ , which is assumed to be constant over the useful range, the SNR at the amplifier output becomes:

$$\text{SNR}_o = \frac{|\mathbf{A}_{B,us}|^2 \nu_{g,\text{eff}}^2}{P_{n,o}} = \frac{|\mathbf{A}_{B,us}|^2 \nu_{g,\text{eff}}^2}{\int_0^\infty |\mathbf{A}_B(2j\pi f)|^2 F(f) |\nu_{r,g}(f)|^2 df} \quad (3.12)$$

Which is lower than  $\text{SNR}_i$ , given by (3.6), since  $P_{n,o}$  includes the total noise of all frequencies and not just the range  $f_L < f < f_U$  used to define in  $P_{n,i}$ . Note that the components following the amplifier are primarily driven by the amplified noise, if the power at the output  $P_{n,o}$  is considerably larger than the useful signal power. That said, the noise of the  $P_{n,o}$  as defined in (3.11) is only of importance if the noise

### 3.1 Amplification

outside the useful range is transmitted. To reduce this signal component we apply a filter that reduces the bandwidth of the signal. Optimally this is a bandpass filter with lower and upper cutoff frequencies at  $f_L$  and  $f_U$ .

If the noise densities of both the signal generator and the amplifier are almost constant in the transfer bandwidth, the noise power at the amplifier output can be approximated by:

$$P_{n,o} \approx F|\nu_{r,g}|^2 \int_0^\infty |\mathbf{A}_B(2j\pi f)|^2 df = F|\nu_{r,g}|^2 |\mathbf{A}_{B,us}|^2 B_r \quad (3.13)$$

Where we defined the *equivalent noise bandwidth* as:

$$B_r = \frac{\int_0^\infty |\mathbf{A}_B(2j\pi f)|^2 df}{|\mathbf{A}_{B,us}(2j\pi f)|^2} \quad (3.14)$$

This means that the area under the plot of the squared magnitude is replaced by the area of rectangle shown in Figure 3.4, i.e. the squared constant gain  $|\mathbf{A}_{B,us}|^2$  times the equivalent noise bandwidth  $B_r$ .

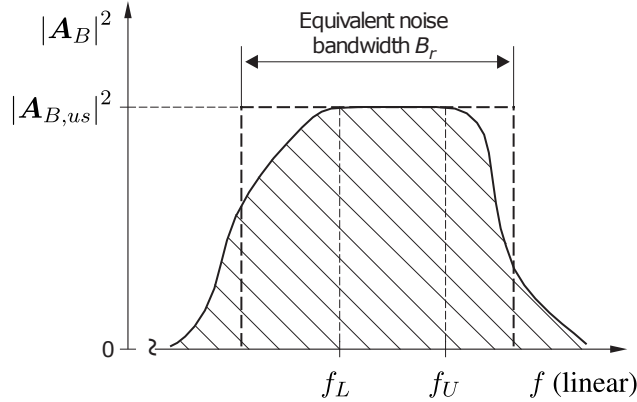


**Figure 3.4:** Equivalent noise bandwidth of an amplifier [13]

### 3.1.3 Instrumentation Amplifier

In resistive sensor applications bridge circuits similar to Figure 2.4b are used. The two outputs of the bridge circuit each carry a signal that enables us to sense a change in resistance differentially. But because the circuit uses a constant supply voltage, a *common-mode*, is present in both signals, i.e. a Direct Current (DC) voltage. If we use standard OPAs for amplification, the differential signal is amplified, while the common-mode voltage receives unity gain. This is a common-mode reduction, the undesirable common-mode is still appearing in the output signal. In contrast, instrumentation amplifiers allow differential signal amplification and all common-mode rejection. It has got a two pin differential input and one single-ended output with respect to a reference terminal.

The Common-Mode Rejection (CMR) is typically specified for the full range common-mode voltage change at a given frequency and source impedance:

$$\text{CMRR} = \left( A_D(f = f_{\text{ref}}) \frac{V_{\text{CM}}}{V_o} \right) \Big|_{Z_S} \quad \text{and} \quad \text{CMR} = 20 \cdot \log_{10} \text{CMRR} \quad (3.15)$$

where

- $A_D$  is the differential gain of the amplifier
- $V_{\text{CM}}$  is the common-mode voltage present at the amplifier inputs
- $V_o$  is the output voltage, when the common-mode signal is applied
- $f_{\text{ref}}$  is the frequency at which the gain is measured
- $Z_S$  is the specified source impedance

Figure 3.5 shows the OPA circuit of a typical instrumentation amplifier. The input buffer amplifiers pass the common-mode voltage through unity gain in both signals. The output signals of the two buffers then connect to the subtractor section where the differential signal is amplified and the common-mode voltage is attenuated. Note that the  $R_G$  resistor is used to set the instrumentation gain, with higher resistance causing lower gains. For more background on instrumentation amplifiers, consult [7]. Because

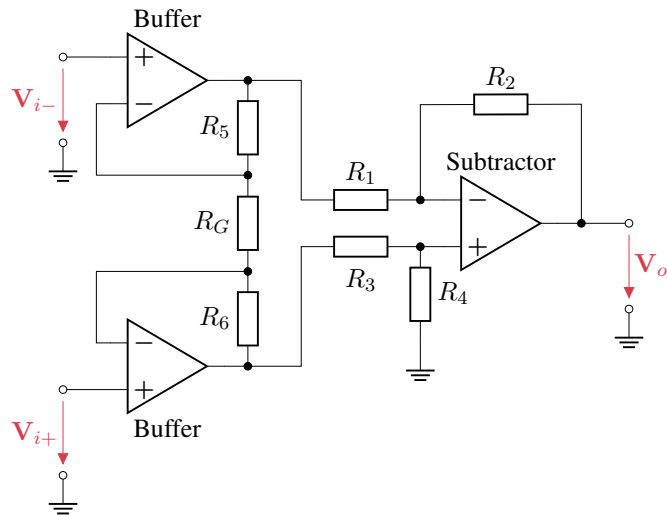


**Figure 3.5:** Typical instrumentation amplifier design

## 3.2 Filtering

Whenever we measure a signal in the real world, it will inherently contain some form of noise. Filtering enables us to cut off contributions to the signal amplitude, that are outside the useful signal frequency bandwidth.

The two main types of filters are analog and digital ones, where the digital filters are more versatile, cost-effective and precise compared to their counterpart. Nevertheless, analog filters are required when dealing with analog signals, i.e. whenever the signal must be bandwidth limited. As described previously, it is advantageous if a signal is bandwidth limited before it is amplified, because we do not want to amplify the noise components of the signal. Furthermore electric devices in the signal chain may be bandwidth limited as well; disturbances of the signal occur due to frequency dependent phase shifts or damping when operating outside these ranges. Namely when digitizing a signal, the additional effect of aliasing may disturb a signal significantly if it contains frequency components above the Nyquist frequency.

We operate at a low frequencies in the frame of this thesis. The useful bandwidth of the lower modes in EMA of MTs range typically between a few ten and a few hundred hertz. Therefore, we focus on a lowpass-filter design, so that there is no miss on the lowest eigenfrequencies. For simplicity, from this point on onward the term bandwidth addresses the upper bandwidth limit, while the lower limit remains near zero. Additionally, the cutoff frequency refers to the lowpass cutoff frequency. For more details on other filter designs we recommend the textbooks for analog electronics and filter design [13], [12] and [18]. The content in this Section is reliant on the theories found in these books.

### 3.2.1 Passive Lowpass Filters

The frequency response of the simplest LPF, as shown in Figure 3.6, can be expressed as

$$H(j\omega) = \frac{v_o}{v_i} = \frac{1}{1 + j\omega RC} \quad (3.16)$$

By replacing  $j\omega$  by  $j\omega + \sigma = s$  one can express the transfer function as

$$H(s) = \frac{\mathcal{L}\{V_o(t)\}}{\mathcal{L}\{V_i(t)\}} = \frac{1}{1 + sRC} \quad (3.17)$$

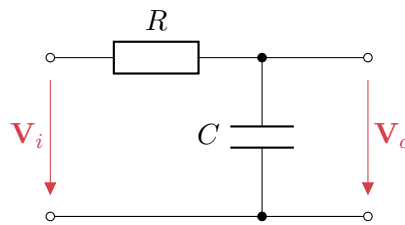


**Figure 3.6:** Simplest passive LPF of first-order

This is the ratio between the Laplace transformed time-domain signals of the output and input respectively. We then generalize the result by normalizing the complex frequency variable  $s$  by defining

$$s_n = \frac{s}{\omega_c} \quad (3.18)$$

For further simplification one can set  $\sigma$  to zero; which is equivalent to assuming sinusoidal form of the input signal. Thus, for  $\sigma = 0$

$$s_n = \frac{j\omega}{\omega_c} = j \frac{f}{f_c} = j\omega_n \quad (3.19)$$

The cutoff frequency of the circuit in Figure 3.6 is  $f_c = 1/(2\pi RC)$ . By definition the normalized complex frequency variable thus becomes  $s_n = 2\pi RC$ . Therefore, the transfer function can be written as

$$H(s_n) = \frac{1}{1 + s_n} \quad (3.20)$$

The magnitude  $|\mathbf{H}(j\omega_n)|$  and phase  $\varphi = \angle \mathbf{H}(j\omega_n)$  of the transfer function for sinusoidal signals are then given by

$$|\mathbf{H}(j\omega_n)|^2 = \frac{1}{1 + \omega_n^2} \quad \text{and} \quad \varphi = \angle \mathbf{H}(j\omega_n) = \arctan \frac{1}{1 + j\omega_n} \quad (3.21)$$

For frequencies  $\omega_n \gg 1$  one can approximate  $|\mathbf{H}| = 1/\omega_n$ . This corresponds to a reduction in gain of 20 dB per frequency decade.

If a sharper cutoff is required,  $N$  LPFs can be connected in series. The Transfer Function (TF) then becomes

$$\mathbf{H}(s_n) = \prod_{i=1}^N \frac{1}{1 + \alpha_i s_n} \quad (3.22)$$

where  $\alpha_i$  are real and positive coefficients and for frequencies  $\omega_n \gg 1$ ,  $|\mathbf{H}| \approx 1/\omega_n^N \propto 1/\omega^N$ . The gain therefore falls off at  $N \cdot 20$  dB per decade. It can be observed that the TF possesses  $N$  real and negative poles. This is characteristic of  $N$ th-order passive  $RC$  LPF.

If we cascade LPFs with identical cutoff frequencies, then

$$\alpha = \alpha_i = \sqrt[N]{\sqrt[2]{-1}} \quad (3.23)$$

which is the condition for which *critical damping* occurs. Each individual cutoff frequency is a factor  $1/\alpha$  higher than that of the filter as a whole.

The TF of the  $N$ th-order LPF has the general form

$$H(s_n) = H_0 \left( 1 + \sum_{i=1}^N c_i s_n \right)^{-1} \quad (3.24)$$

where  $c_i$  are real and positive coefficients and the order of the filter is equal to the highest power of  $s_n$ . By rewriting the denominator in factored form and allowing complex poles, one denotes Equation 3.24 as

$$H(s_n) = \frac{H_0}{(1 + a_1 s_n + b_1 s_n^2)(1 + a_2 s_n + b_2 s_n^2) \cdots} \quad (3.25)$$

where  $a_i$  and  $b_i$  are real and positive coefficients and  $b_1 = 0$  for odd orders  $N$ .

The frequency response can be optimized to different theoretical aspects by setting the coefficients  $a_i$  and  $b_i$ . As a consequence of these optimizations, complex poles arise, that cannot be realized by blocks of

### 3.2 Filtering

passive  $RC$  filters. It is possible to meet the optimized conditions by using  $LCR$  filters with the simplest example shown in Figure 3.7, where

$$H(s) = \frac{1/(LC)}{s^2 + \frac{R}{L}s + \frac{1}{LC}} \quad \text{and} \quad f_c = \frac{1}{2\pi\sqrt{LC}} \quad (3.26)$$

This design does not pose any difficulties when opting for high cutoff frequencies. But it is apparent, that one requires the use of large capacitances as well as large inductances for low cutoff frequencies. And because large inductances are unwieldy and have poor electrical properties, an active filter design is better suited for low cutoff frequencies. With these designs the use of inductances are avoided by the addition of active elements, namely OPAs, to the  $RC$  network.

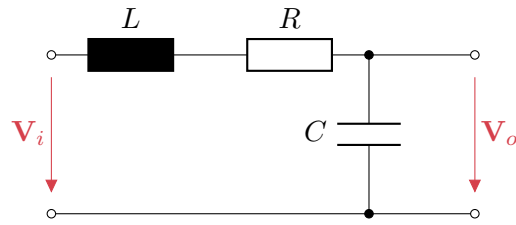


**Figure 3.7:** Passive second-order LPF, LRC circuit

### 3.2.2 Optimizations of Lowpass Filters

Following Tietze [13], we take the *standard form* of the second-order LPF into consideration, where:

$$H(s_n) = \frac{H_0}{1 + a_1 s_n + b_1 s_n^2} = \frac{k}{1 + \frac{s_n}{Q} + s_n^2} = \frac{k}{1 + 2\zeta s_n + s_n^2} \quad (3.27)$$

$$Q = \frac{1}{2\zeta} = \frac{b_1}{a_1} \quad (3.28)$$

where  $k$  is the gain factor and  $Q$  is the quality factor respectively  $\zeta$  the damping ratio. In the case of unity gain,  $k = 1$ , one can see that the two poles are given by:

$$p_{1,2} = (-\zeta \pm \sqrt{\zeta^2 - 1})\omega_n \quad (3.29)$$

and that the poles are...

- real if  $\zeta \geq 1$
- complex if  $0 < \zeta < 1$
- imaginary if  $\zeta = 0$
- in the right half plane and unstable with  $\text{Re}\{p\} > 0$  if  $\zeta < 0$

If we now take a look at the second-order system used to describe the accelerometer dynamics in (2.2) and replace the static sensitivity  $K$  with the gain factor  $k$  the system dynamics are equal and one can see the influence of the damping factor on the system behavior in Figure 2.3. Many filter designs expose this configurability of a second order systems. Because of parameters  $k$  and  $\zeta$  respectively  $Q$  to tune the filter behavior and gain different optimization points targeted. Moreover, when connecting multiple second-order filters in series to realize higher-order filters with steeper roll-offs, the individual second-order filter parameters can be tuned to match three distinct optimization points:

- The *Chebyshev* filter is optimized to have a steep roll-off rate but shows ripple in the pass- and stopband.
- The *Butterworth* filter is optimized to have the most stable gain at the passband but has a poor roll-off rate.
- The *Bessel* filter is optimized to have the most stable phase response, which is critical for fast signal level changes. The caveat comes in form of the poorest roll-off of all filters, when compared at same order.

The influence of the order on the filter gain can be seen in Figure 3.11. Above, the passband refers to frequency contributions below the cutoff frequency and the stopband is defined depending on the application. If one expects high noise densities directly above the cutoff frequency, the stop band needs to be defined at a low gain and the roll-off of the filter must be designed to be steep, whereas if some application only allows small phase shifts, the latter cannot be achieved by a high order filter. The definition of the cutoff frequency is more consistent. For most filters the cut-off frequency is reached, when the gain falls short by 3 dB, i.e. when the filter halves the squared gain, which in turn is proportional to the power transmission. An exception is the Chebyshev filter. Here it is common to define the cutoff the point where the filter roll-off reaches minus the maximally allowed ripple gain in decibel, see Figure 3.8. Note that given the three optima, any hybrid filter design between the Chebyshev and the Butterworth as well as between the Butterworth and Bessel is possible too.

### 3.2 Filtering

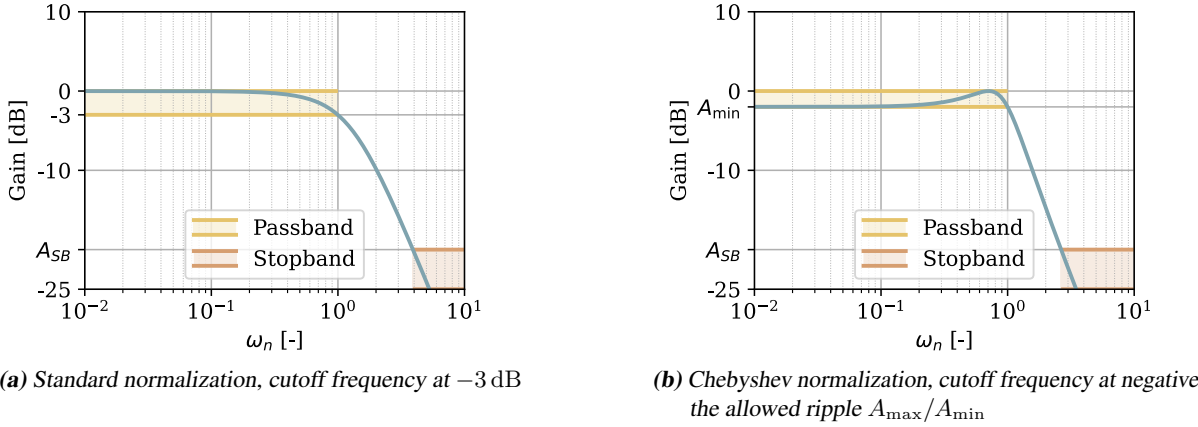


**Figure 3.8:** LPF Pass- and Stopband, where the passband is defined by  $\omega_n < 1$  and the stopband is chosen depending on the application (usually starting at  $-20 \dots -160 \text{ dB}$ )

When comparing the step and impulse responses in Figure 3.9 and Figure 3.10, it becomes apparent that one must trade better frequency-cutoff with worse signal response in the time domain. This is because the change in phase over the frequency, i.e. the group delay, is almost constant in the Bessel filter, whereas the Chebyshev optimization, tuned to maximum gain roll-off speed, induces fast changes in the phase. This causes the undesired swinging in the time signals. The phase responses can be compared in Figure 3.12. A more in depth look at the group delay is given in the following description of the Bessel filter.

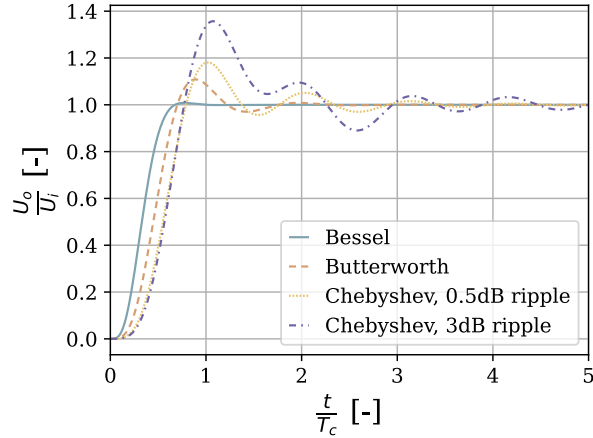


**Figure 3.9:** Step response of fourth-order LPF — Note, that the Chebyshev filter is represented with the cutoff frequency at  $-3 \text{ dB}$  for comparability.

Until now we described all-pole LPFs, i.e. no nodes are present in the filter system, as can be seen in the TF (3.25). With filter designs that include nodes, one can realize sharper cutoffs without increasing the phase shift. Generally more complex filter curves are possible at the cost of more unstable behavior and more complex filter design. Due to these disadvantages their behavior is not as reliable as the filters listed before. Therefore they were not considered during this thesis. For more background on these filters, also called *elliptic-function* filters, we advice to take look at the textbook [18].

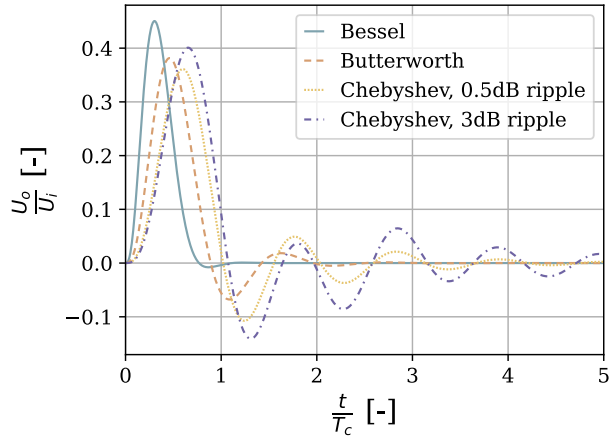


**Figure 3.10:** Impulse response of fourth-order LPF — Note, that the Chebyshev filter is represented with the cutoff frequency at  $-3$  dB for comparability.

### Butterworth Lowpass Filter

From the general solution in Equation 3.24 the squared absolute gain in LPFs takes the form

$$|\mathbf{H}(\omega_n)|^2 = H_0^2 \left( 1 + \sum_{i=1}^N k_{2i} \omega_n^{2i} \right)^{-1} \quad (3.30)$$

where odd powers of  $\omega_n$  do not occur, since  $|\mathbf{H}|^2$  must be an even function. In Butterworth LPFs the function  $|\mathbf{H}|^2$  must be maximally flat at  $\omega_n < 1$ , i.e. for frequencies below the cutoff frequency. This condition is best met if we only keep the highest order term, since lower order terms contribute the most to the denominator at low frequencies, decreasing the gain. Hence, for Butterworth LPFs

$$|\mathbf{H}(\omega_n)|^2 = \frac{H_0^2}{1 + k_{2N} \omega_n^{2N}} \quad (3.31)$$

where  $k_{2N} = 1$  due to the normalizing condition, which states that the square of the gain is reduced by 3 dB at  $\omega_n = 1$ , i.e.  $|\mathbf{H}(\omega_n = 1)|^2 = |\mathbf{H}(\omega_n = 0)|^2/2$ .

When implementing a Butterworth LPF, one needs to consider the complex gain  $\mathbf{H}$  involved in Equation 3.31. It can be determined by solving for coefficients  $c_i$  in Equation 3.24, given the squared gain of Equation 3.31. It is then possible to solve the transfer function analytically by combining complex conjugate poles. In the solution, we obtain the coefficients  $a_i$  and  $b_i$  of the quadratic expression in Equation 3.25

even order  $N$ :

$$\begin{aligned} a_i &= 2 \cos \frac{(2i-1)\pi}{2N} & \text{for } i = 1, 2, \dots, \frac{N}{2} \\ b_i &= 1 \end{aligned}$$

odd order  $N$ :

$$\begin{aligned} a_2 &= 1, & a_i &= 2 \cos \frac{(i-1)\pi}{N} & \text{for } i = 2, 3, \dots, \frac{N+1}{2} \\ b_1 &= 0, & b_i &= 1 \end{aligned}$$

### 3.2 Filtering

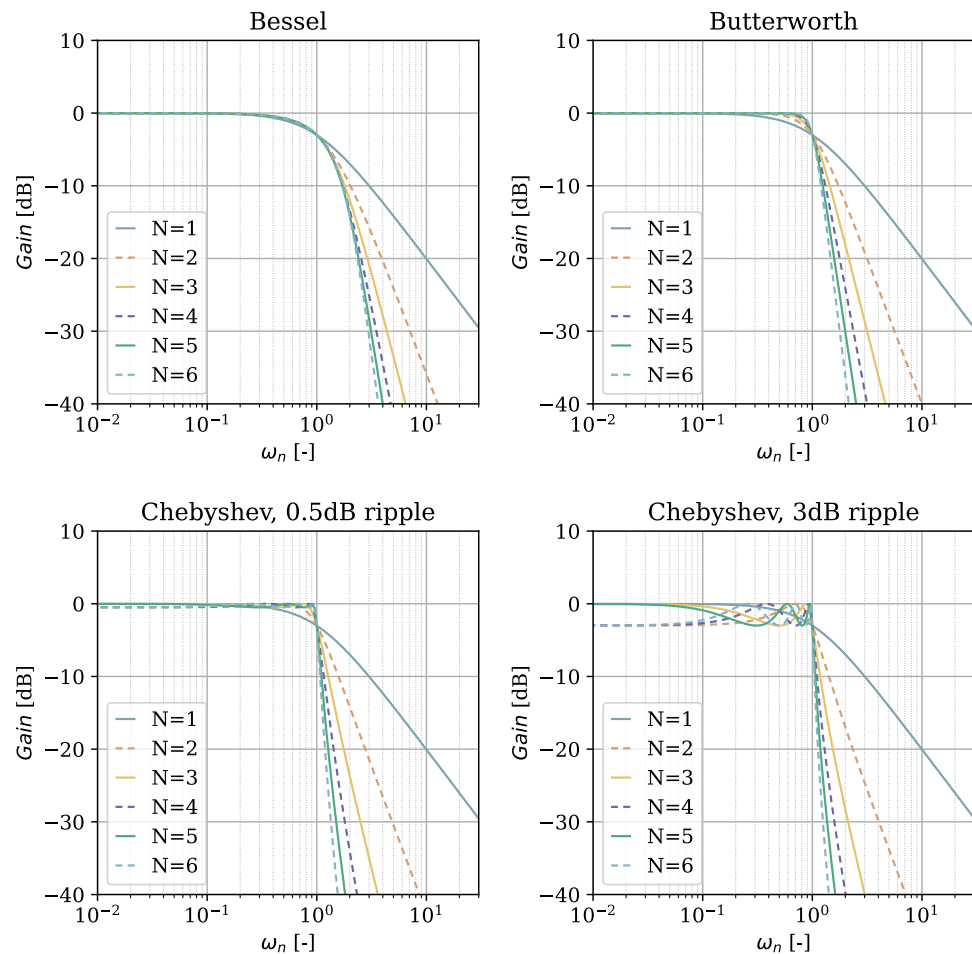


**Figure 3.11:** Influence of LPF order  $N$  on the amplitude of the frequency response — Note, that the Chebyshev filter is represented with the cutoff frequency at -3 dB for comparability.

## Chebyshev Lowpass Filter

In the passband the Chebyshev LPF is allowed to have a predetermined ripple. The characteristic of Chebyshev polynomials is, that the ripple ripples are constant, i.e. their local extrema in the gain plot can be connected by two horizontal lines that are displaced by the predetermined ripple.

$$T_N(x) = \begin{cases} \cos(N \arccos x), & \text{for } 0 \leq x \leq 1 \\ \cos(N \operatorname{arccosh} x), & \text{for } x > 1 \end{cases} \quad (3.32)$$

To get the LPF from these Chebyshev polynomials, we define

$$|\mathbf{A}|^2 = \frac{k A_0^2}{1 + \varepsilon^2 T_N^2(x)} \quad (3.33)$$

where  $A_0$  is the so called DC- or zero-gain and the constant  $k$  is chosen such that, for  $x = 0$ , the square of the gain  $|\mathbf{A}|^2$  becomes  $A_0^2$ . If  $N$  is even, this means  $k = 1$  and if  $N$  is odd, we set  $k = 1 + \varepsilon^2$ ; where the latter is a measure of the ripple and is given by

$$\frac{A_{\max}}{A_{\min}} = \sqrt{1 + \varepsilon^2} \quad (3.34)$$

and

$$\left. \begin{array}{l} A_{\max} = A_0 \sqrt{1 + \varepsilon^2} \\ A_{\min} = A_0 \end{array} \right\} \quad \begin{array}{l} \text{if } N \text{ is even} \\ \text{if } N \text{ is odd} \end{array} \quad \left. \begin{array}{l} A_{\max} = A_0 \\ A_{\min} = A_0 / \sqrt{1 + \varepsilon'^2} \end{array} \right\} \quad \begin{array}{l} \text{if } N \text{ is odd} \\ \text{if } N \text{ is even} \end{array} \quad (3.35)$$

Once  $|\mathbf{A}|^2$  is determined, the complex gains can be calculated. However, it is easier to derive the poles of the transfer function directly of the Butterworth filters. By combining the complex conjugates the coefficients  $a_i$  and  $b_i$  in (3.25) are determined:

$$\left. \begin{array}{l} b'_i = \frac{1}{\cosh^2 \gamma - \cos^2 \frac{(2i-1)\pi}{2N}} \\ a'_i = 2b'_i \cdot \sinh \gamma \cdot \cos \frac{(2i-1)\pi}{2N} \\ b'_1 = 0 \\ a'_1 = 1 / \sin \gamma \\ b'_i = \frac{1}{\cosh^2 \gamma - \cos^2 \frac{(i-1)\pi}{N}} \\ a'_i = 2b'_i \cdot \sinh \gamma \cdot \cos \frac{(i-1)\pi}{N} \end{array} \right\} \quad \begin{array}{l} \text{if } N \text{ is even and} \\ \text{for } i = 1 \dots \frac{N}{2} \\ \text{if } N \text{ is odd and} \\ \text{for } i = 2 \dots \frac{N+1}{2} \end{array}$$

where  $\gamma = \frac{1}{N} \operatorname{arcsinh} \frac{1}{\varepsilon}$

The obtained coefficients  $a'_i$  and  $b'_i$  define a Chebyshev filter at the cutoff frequency  $\omega_x$ , which the gain assumes the value  $A_{\min}$  for the last time. For easy comparison with other filter types we want to evaluate the filter at a cutoff frequency where the gain is  $-3$  dB. For this we multiply the normalized frequency  $s_n$  with a real constant  $\alpha$ , changing the quadratic expressions in the denominator of (3.25) to

$$(1 + a'_i \alpha s_n + b'_i \alpha^2 s_n^2)$$

### 3.2 Filtering

Next, we evaluate  $\alpha$ , so that the gain value is  $1/\sqrt{2} \hat{=} -3 \text{ dB}$  at the normalized frequency  $s_n = j$ . The coefficients for the filter with cutoff frequency pass through at  $-3 \text{ dB}$  can then be determined by multiplication with the constant.

$$a_i = \alpha a'_i \quad \text{and} \quad b_i = \alpha^2 b'_i \quad (3.36)$$

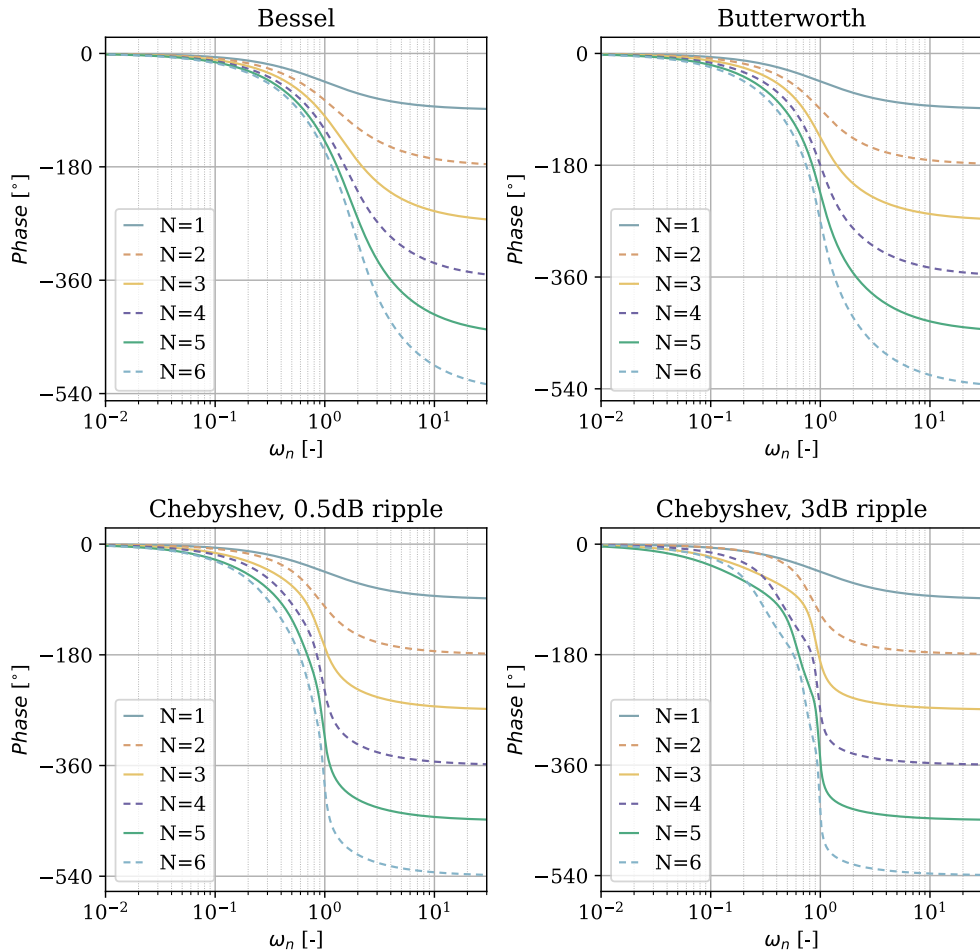


**Figure 3.12:** Influence of the LPF order  $N$  on the phase of the frequency response — Note, that the Chebyshev filter is represented with the cutoff frequency at  $-3 \text{ dB}$  for comparability.

## Bessel Lowpass Filter

In the step and impulse response, Figure 3.9 and 3.10, the Butterworth and Chebyshev filters show considerable overshoot. With the Bessel or also called Thomson filter we aim to mitigate this effect in order to create smooth response curves. It can be shown, that best square-wave responses are obtained when the *group delay* of the filter is constant with respect to the frequency. The condition for the lowpass Bessel filter therefore sets the group delay in the passband maximally flat. The group delay  $t_{gr}$  is defined as the negative of the change in phase shift due to frequency change.

$$t_{gr} = -\frac{d\varphi}{d\omega} \quad (3.37)$$

Often we use the normalized group delay for calculations

$$T_{gr} = t_{gr}\omega_c = 2\pi t_{gr}f_c = 2\pi \frac{t_{gr}}{T_c} \quad (3.38)$$

And given that the reciprocal of the cutoff frequency is by definition  $T_c = 2\pi/\omega_c$

$$T_{gr} = -\omega_c \frac{d\varphi}{d\omega} = -\frac{d\varphi}{d\omega_n} \quad (3.39)$$

As an example, we consider the gain of a second-order LPF given by (3.25) and assume sinusoidal signals, i.e.  $s = j\omega$ . The phase shift of this system is

$$\varphi = -\arctan \frac{a_1\omega_n}{1 - b_1\omega_n^2} \quad (3.40)$$

Thus by calculating the negative of the derivative with respect to the normalized frequency, we get the normalized group delay

$$T_{gr} = \frac{a_1(1 + b_1\omega_n^2)}{1 + (a_1^2 - 2b_1)\omega_n^2 + b_1^2\omega_n^4} \quad (3.41)$$

For small frequencies, where  $\omega_n \ll 1$ , we can neglect the fourth order terms and this simplifies to

$$T_{gr} = a_1 \frac{1 + b_1\omega_n^2}{1 + (a_1^2 - 2b_1)\omega_n^2} \quad (3.42)$$

Now  $T_{gr} = f(\omega_n^2)$  and we can find the coefficient configurations where it becomes independent of  $\omega_n^2$ , that is

$$b_1 = a_1^2 - 2b_1 \quad \text{or} \quad b_1 = \frac{1}{3}a_1^2 \quad (3.43)$$

A second equation to determine the coefficients is given, when we set the gain at the cutoff frequency to  $-3$  dB, i.e.  $|A|^2 = 1/2$  at  $\omega_n = 1$ .

$$\frac{1}{2} = \frac{1}{(1 - b_1)^2 + a_1^2} \quad (3.44)$$

The calculations of higher order filters become more involved, since a system of nonlinear equations arises. But using a different approach one can find a recursion formula for the coefficients in (3.24).

$$c'_1 = 1 \quad \text{and} \quad c'_i = \frac{2(N - i + 1)}{i(2N - i + 1)} c'_{i-1} \quad \text{for } i = 2 \dots N \quad (3.45)$$

### 3.2 Filtering

But note, that this approach gives the coefficient for 3 dB frequency cutoffs at  $\omega_n = 0$ . To find the coefficients at for a usable cutoff frequency, we apply the same approach as we did with the Chebyshev coefficients. For that we rewrite the equation in form of (3.25) to get the second-order filter coefficients  $a'_i$  and  $b'_i$ , apply the transformation  $s_n = \alpha j\omega_n$  and solve for  $\alpha$ . The coefficients  $a_i$  and  $b_i$  can then be calculated with (3.36).

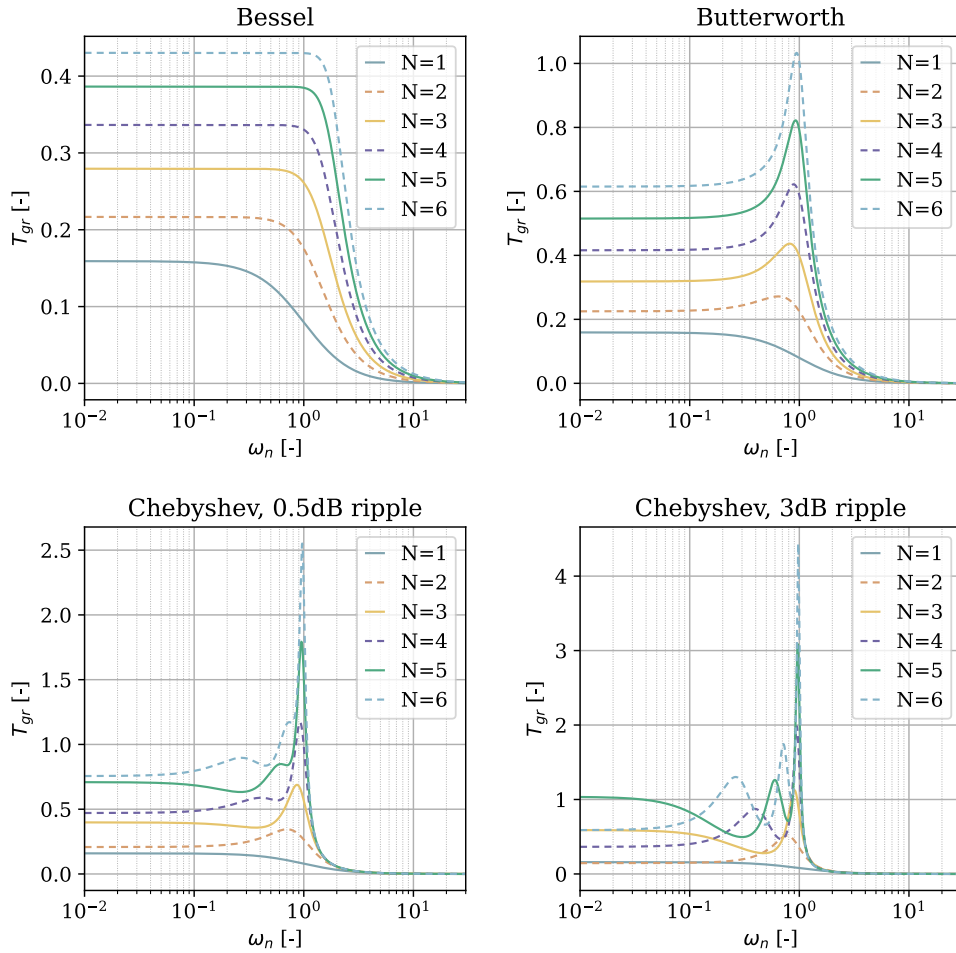


**Figure 3.13:** Influence of the LPF order  $N$  on the group delay of the frequency response — Note, that the Chebyshev filter is represented with the cutoff frequency at  $-3$  dB for comparability.

### 3.2.3 Active Filter Topologies

Depending on the desired filter optimization target, one can choose the best suited topology to approach its TF. First-order topologies are the noninverting and the inverting LPF, see Figure 3.14. Note that the negative sign in the TF of the inverting amplifier generates a  $180^\circ$  phase shift from input and output. Furthermore, at unity gain both  $R_1$  and  $R_2$  tolerances have an influence on the gain; therefore the noninverting impedance LPF is preferred if one is looking for high unity gain accuracy.

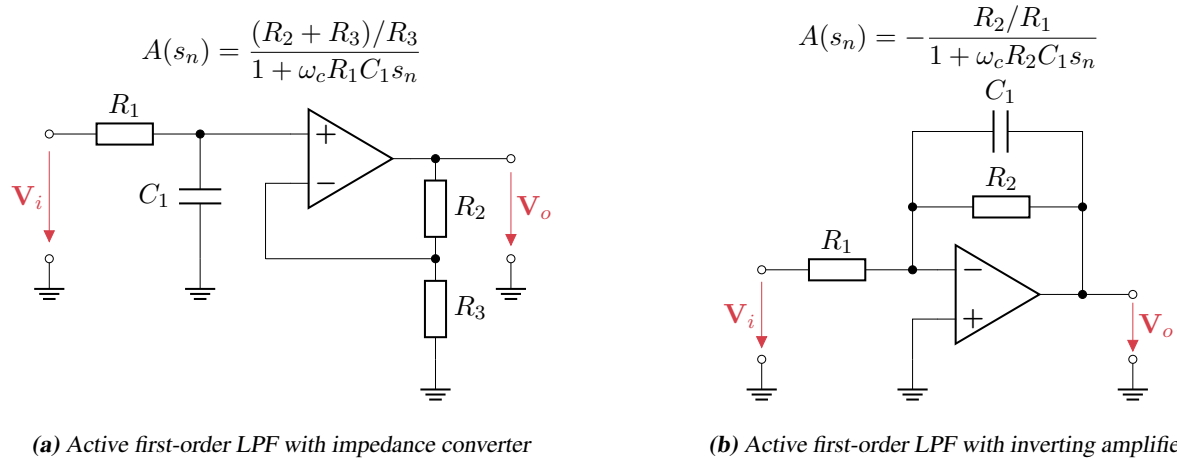


**Figure 3.14:** First-order lowpass filter topologies

The Sallen-Key topology is a common building block for filters. It is best used for applications that do not require sharp cutoffs. Since it is difficult to generate large Q-factors with this design.

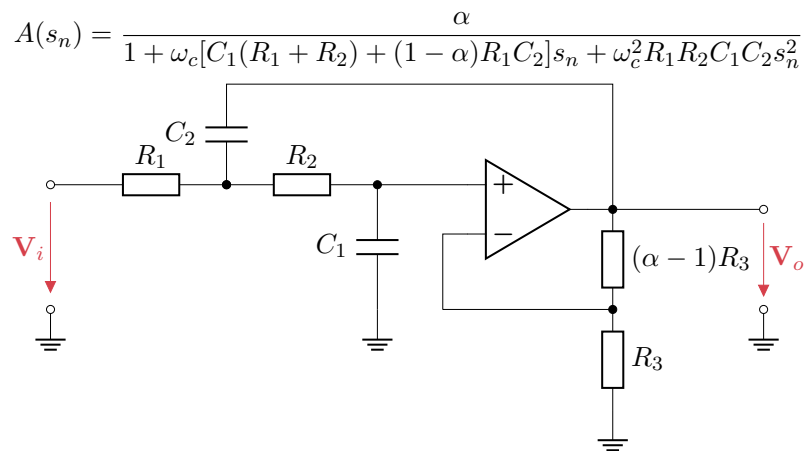


**Figure 3.15:** Active second-order LPF with single positive feedback, Sallen-Key

### 3.2.4 Anti Aliasing Filter

The Anti Aliasing Filter (AAF) is used ahead of ADCs to reduce the signal bandwidth. More precisely, it aims to reduce the aliasing effect, i.e. the artificial distortion of signals, that occurs when sampling at a finite frequency. The effect that aliasing can have on a signal is visualized in Figure 3.16. Here two analog sinusoidal signals are sampled at the same sampling frequency  $f_s$ . The digitized signal will always be an approximation of the analog one, but it is clear that the signal with  $f < f_{\max}$  has a better approximation in its digital form, and most importantly, it is an approximation of same frequency in contrast to the signal with  $f > f_{\max}$ .

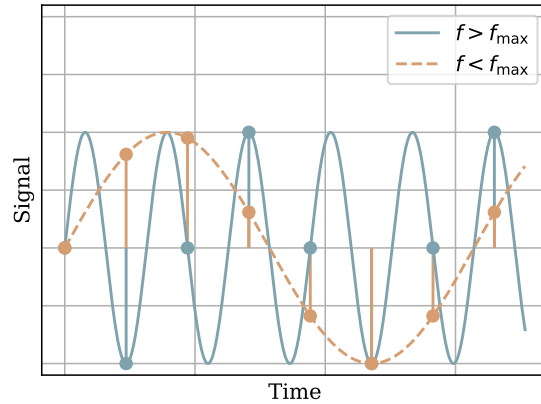


**Figure 3.16:** Aliasing effect — Note, that two analog sinusoidal signals of different frequencies are shown and sampled at the same frequency  $f_s$ . Interpolating the discrete points gives the respective digital signals, where the signal with frequency  $f < f_{\max}$  gives a good approximation of its analog form and the signal with frequency  $f > f_{\max}$  connects to a lower frequency signal in its digital form.

More specifically, when we take the Fourier Transform (FT) of the signal with  $f > f_{\max}$  we see a peak of the absolute amplitude at a new frequency  $f_d \leq f_s < f$ . Similarly, when using input signals with multiple frequency components, the signal gain distorted by components from the domain  $f > f_{\max}$ . This distortion is the result of overlapping signal components, which makes them indistinguishable. This is called aliasing.

For signals that are bandwidth limited, i.e their FT is zero outside a finite region, the *Nyquist-Shannon* sampling theorem finds that if those signals are sampled at  $f_s = 2f_{\max}$ , where  $f_{\max}$  is the highest frequency component, it is completely determined. Therefore, we want to cut off all frequency components above  $f_s/2$  before digitizing any signal.

### 3.3 Analog to Digital Conversion

The ADC shows internal noise that can be categorized into two uncorrelated main sources. The quantization noise and the thermal noise. The total internal noise can thus be expressed as the Euclidean norm of these two sources.

$$N_{\text{ADC}} = \sqrt{N_{\text{ADC,Thermal}}^2 + N_{\text{ADC,Quantization}}^2} \quad (3.46)$$

Quantization noise is present due to the process of mapping an infinite number of possible electrical signal values in an analog signal to a finite number of digital codes. Subsequently, any digital output corresponds to an infinite number of analog inputs within range of the output value, plus and minus half the Least Significant Bit (LSB) size,  $s_{\text{LBS}}$ . One can decrease quantization noise by choosing a higher resolution ADC.

$$s_{\text{LBS}} = \frac{V_{\text{FSR}}}{2^m} \quad (3.47)$$

where

- $V_{\text{FSR}}$  is the full-scale range of the analog input value and
- $m$  is the resolution in number of bits

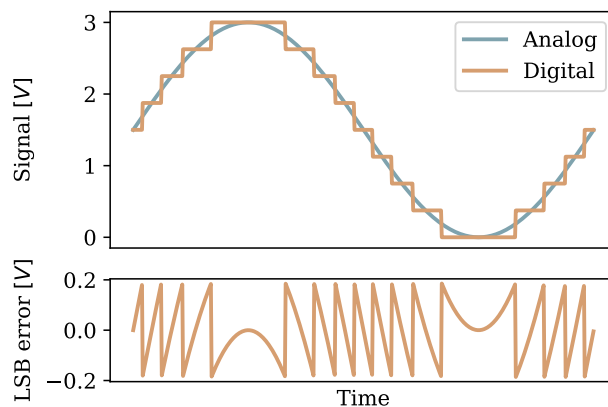


**Figure 3.17:** ADC — Analog input, digital output and LSB error waveform with  $s_{\text{LBS}} = 375 \text{ mV}$  [6]

Thermal noise is a phenomenon inherent in all electrical components. Because of this, it is a function of the device design and cannot be affected by the embedded system designer. Typically, one assumes the thermal noise to have a Gaussian distribution.

Depending on the relative noise contributions of each source, we divide ADCs into two extremes. Low- and high resolution ADCs. Characteristic for a low-resolution ADC is that  $N_{\text{ADC,Quantization}} \gg N_{\text{ADC,Thermal}}$ . Here the quantization noise dominates because of the large LSB size. Typically, starting above 16 bit resolution we decimates the LSB so that the thermal noise becomes dominant. Within the low-cost system operate primarily with low-resolution ADCs.

### 3.3 Analog to Digital Conversion

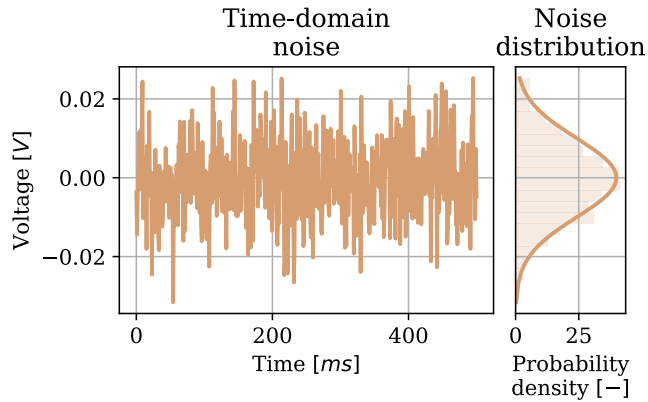


**Figure 3.18:** ADC — Thermal noise in the time domain with Gaussian probability density [6]

ADC Topology	Data rates / MS/s	Resolution / bit	Benefits
SAR	$\leq 4$	$\leq 18$	<ul style="list-style-type: none"> <li>• simple implementation</li> <li>• no latency</li> <li>• low power</li> </ul>
delta-sigma	$\leq 10$	$\leq 28$	<ul style="list-style-type: none"> <li>• high resolution</li> <li>• high integration</li> </ul>

**Table 3.1:** ADC topologies

#### 3.3.1 Topologies

Successive-Approximation (SAR) ADCs have a low-power consumption and are available in very small packages. This makes them the preferred option for mobile devices as well as general purpose applications and data acquisition systems. An additional advantage of the SAR topology is the negligible or zero latency. Its power consumption is proportional to the sampling rate.

The delta-sigma ADCs offer the highest-resolution and are generally preferred in precision applications. Because they are highly integrated, they replace many components of a data acquisition system. In this topology a digital filter is included, typically optimized for the application. Its disadvantages are medium power consumption and cycle latency.

# 4

## Data Acquisition and Software

### 4.1 Data Acquisition

The DAC system developed in this thesis is an open source Arduino based system consisting of multiple microcontrollers. All signal channels are transmitted to a central microcontroller before passing to a computer that serves as visualization and analysis tool.

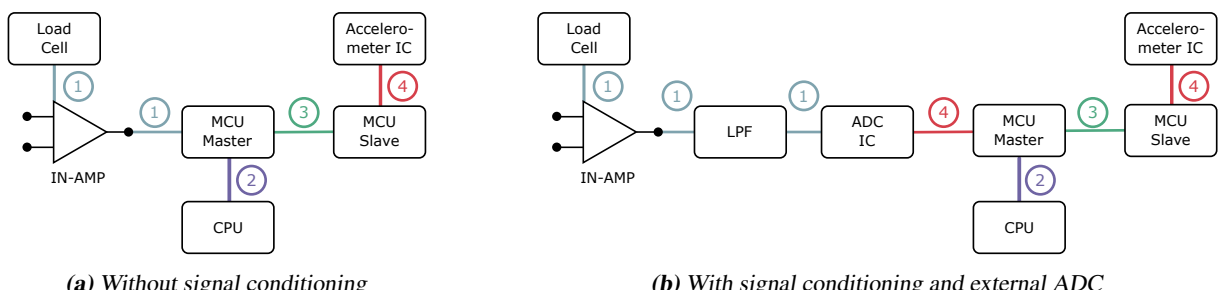


**Figure 4.1:** DAC-system building blocks — note that 4.1a has been realized, but 4.1b has not been implemented yet, due to communication issues between the devices

Interfaces
① : Analog Signal
② : Universal Serial Bus (USB)
③ : Recommended Standard (RS)-485
④ : SPI

**Table 4.1:** Legend to Figure 4.1

## 4.1 Data Acquisition

### 4.1.1 Building Blocks

Building blocks are the main components used in the DAC signal chain. Additional components that are required to enable the stable operation of the building blocks are not shown; e.g. the RS-485 drivers.

Because the of accelerometer IC output interfaces it is not possible to connect all sensors directly to one MCU that acts as a DAC. We need to transform the signal to a different interface. A low-cost and versatile method to achieve this, is to use a MCU for each accelerometer IC. These read the sensor IC registers and communicate to the MCU master. The master, on the other hand, acts as a passthrough and transmits the data to the Central Processing Unit (CPU). In the setup used, it also reads out the LC signal. Table 4.2 lists the MCUs used during this thesis.

The analog signal output of the LC needs to be amplified to match the input range of the ADC. To gain the maximum resolution, this depends on the expected input range. For an additional resolution benefit, than offered by the microcontroller embedded ADC one can include an external ADC IC upstream of the MCU. Additionally, we use a LPF in Figure 4.1b. The LPF following the LC is mainly used to cut off noise components of the signal. But, because the accelerometers have an integrated AAF at usually 800 Hz, the lowpass filter also limits the bandwidth of the hammer signal to a bandwidth of up to 800 Hz. In that sense it also acts as a AAF for the consecutive ADC. In other words, we limit the systems bandwidth to a sampling rate of 1600 Hz, the maximum sampling rate of the slowest sensor. Therefore, we use the maximal possible bandwidth according to Nyquist.

As instrumentation amplifier the AD627 from Analog Devices has been implemented. All microcontroller PCBs used during this thesis are listed in Table 4.2.

Name	Core	ADC-Resolution / bit	Operating Voltage / V	Clock Speed / MHz	Flash Memory / kByte	SRAM / k Byte
Arduino Due	AT91SAM3 ARM Cortex	12	3.3	84	512	96
Teensy 3.2	MK20DX256VLH Cortex-M4	13 (16 bit-values)	3.3	72	256	64
Robotdyn Blackpill	STM32F103C8 Cortex-M3	12	3.3	72	64	20

**Table 4.2:** List of MCUs used in this work

### 4.1.2 Interfaces

The interfaces are the connections and protocols between the different building blocks of the DAC system. The interfaces are chosen based on the sensors used and the expected data rate at the required cable length between each section. I.e.:

- Between the analog LC and the external ADC in Figure 4.1b and the MCU integrated ADC in Figure 4.1a respectively the signal transmission is analog.
- The register of the accelerometer IC is accessed via SPI
- The communication between MCUs is rooted in RS-485 differential transmission to accommodate for signal transmission over cable lengths greater than 10 m and uses a specialized protocol to keep data packages as small as possible.
- Between the MCU and the CPU USB transmits data using the serial class of the Arduino software.

Data rates and package sizes are critical when sampling at high frequencies.

With RS-485 data can be transmitted over distances of no less than 100 km at a data rate of 1 kbit/s. At 1200 m cable length we can reach data rates of around 100 kbit/s. In our range of application, i.e. a few tens of m, we can expect data rates of 1 Mbit/s, thus representing the bottle neck in the digital data chain. If we then transmit 80 bit acceleration measurements (see Figure 4.2) at 1.6 kHz we stay below this expected limit by a safety factor of more than 10. The arduino the serial package parses all data as human readable code, specifically American Standard Code For Information Interchange (ASCII). In this format every digit of integer values is passed as 8 bit-value. Which means that a 32 bit timestamp and every single axis acceleration are passed as ten 8 bit-values and six 8 bit-values respectively. This increases the size of an accelerometer package to 624 bit, which in turn reduces the safety factor to approximately 1. It is clear that one cannot use human readable code to transmit the data and guarantee stability at the required sampling rate.

### MCU communication protocol

The communication protocol between MCU and MCUs and between MCU and computer was developed for this project.

<b>&lt;[ (reg) (#bytes) (data) ]&gt;</b>
_____
<[/> : Start-/End-bytes, represented as ASCII
(reg) : Registry/Address of the transmission
(#Bytes): Number of bytes in transmission
(data) : Data to transmit

**Table 4.3:** Protocol used to communicate between two MCU's and between MCU and computer

## 4.1 Data Acquisition

### 4.1.3 Dataflow

The dataflow between the MCUs is sequential and all data is passed to a central MCU, called master, before we streamline it to the CPU. The master cycles through all connected MCUs, performing a data request, hold and receive action. As soon as a slave MCU gets a request, it transmits a data package from its buffer. The master, now receiving the data package, will throughput the signal to the CPU, where the data is stored. By the end of this process the master will jump to the next slave.

All measurements consist of a 32 bit-timestamp and the measured values and are pushed into a First In, First Out (FIFO) buffer in the flash memory of the MCU, directly connected to the sensor. Bundled data packages are then pulled from the buffer and translated into the transmission code as defined in Table 4.3. In Figure 4.2 the data flow is represented by a system that is using only one slave MCU, displayed in violet.

Time synchronizations are executed in form digital data exchange, by synchronizing the timestamps before a complete measurement. The sensor measurements themselves are conducted as soon as ready to benefit of the sensors maximum measurement frequency. With this method, no data bandwidth is used between measurement cycles for clock synchronization, but it comes with three caveats. Firstly, every MCU runs on its own clock cycle. Measurements are conducted whenever the individual time interval after the clock is exceeded. These time intervals are matched by sharing the master timestamp with the ones of the slave programmatically. The slave timestamps are then tuned to same value during a setup process. But after the synchronization the Gaussian distributed deviations to the intervals accumulate, ultimately yielding unknown time-shifts to the signals.

Measurements are packaged due to the time the master requires to change the communication to another slave. During these switches no data is transmitted eventually limiting the data rate of the system.

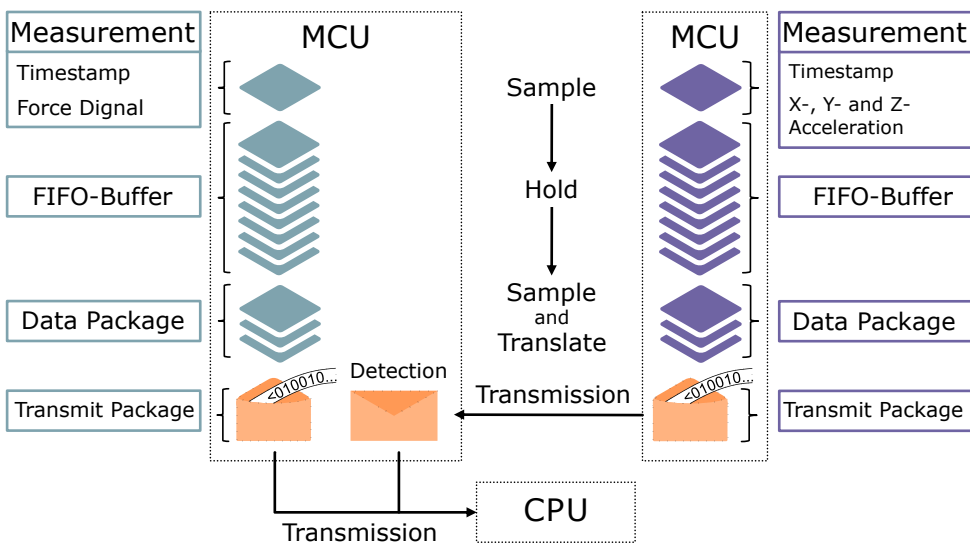


**Figure 4.2:** Data flow between two MCUs and the CPU

## 4.2 Software

The software developed during this project is split into the Arduino software running on the MCUs and a python based tool to receive and visualize the data via USB.

For the instrument to work, some functions are required, while other desired functions are tools that simplify the workflow during measurements and facilitate bug fixes in the software.

The requirements to the software tools are:

1. Read out accelerometer and LC data at the maximum sample speed of the accelerometer IC.
2. Synchronize measurements timestamps.
3. Initialize measurement by hammer impulse.

The desired software tools are:

4. Generate continuous real time output of measurement data.
5. Track data transfer via USB.

### 4.2.1 Implementation

For data communication, all data software used in this project use a standardized input and output of the package format described in Table 4.3; where the addresses are used as identifiers.

#### Common Addresses

Addresses are identified by a parser that identifies the instruction contained in the address. Every device is assigned to handle predefined addresses accordingly. That is, it processes the instruction or it transmits the data package to then next device. Every data package keeps its address as defined in Table 4.3 from start to destination. A measurement package, for example includes multiple measurements in the data block and has an address specific to the measurement sensor, with its destination to the CPU, whereas a command from the computer application has a destination address to one specific MCU; all MCUs inbetween the two devices transmit the data as is. For this reason, although the parser is defined by the same class in every device, it requires an additional identification to detect on which device the parser is running.

#### Microcontroller Software

The software running on the MCU is programmed in the Arduino programming language and uploaded via bootloader. This way, the software can be uploaded by a serial interface but, additionally to the software itself, some of the flash memory is reserved for the bootloader. The remaining memory is used during operation is used for a digital FIFO buffer. Because all used MCUs are using one core only, parallel data transfer is not possible and the data must be merged and serialized at the master MCU. Both the parser and the buffer add an overhead to the cyclic running program on the MCU that potentially limits the communication speed.

### Computer Software

The software on the computer runs in python. As a key module that enables the communication between the running python script and the serial port the pyserial has been used. The software tools are able to identify, store and visualize the captured data.

#### 4.2.2 Challenges

##### Time Synchronization

The time synchronization between the MCUs is handled on software level. The master sends its current clock as a data package to the slaves and they adapt their clocks accordingly. This is the simplest approach apart from an interrupt and can be conducted with higher accuracy when estimating the transmission duration. For example, when using a feedback loop, where the slave directly returns the sent signal, the master can estimate the transmission duration by dividing the duration since the transmitted message minus the slave processing time in two. In this manner it then sends the master time minus the estimated transmission duration to the slave. The caveat of this approach is, that no real synchronization but only estimated timestamp synchronizations are realized. During the sensors and their respective MCUs run on different clock cyclers, that are prone to deviate from another. Additionally, the timestamps have a considerable impact on the data bandwidth during measurements.

Until now no better solution has been implemented into the software. The time synchronization might be reconsidered altogether and moved to the physical layer, to reduce the bandwidth of the measurement package. For example, with clock synchronization the MCU clocks themselves would match the master clock. Synchronization timestamps are no longer needed but the slaves must be connected by a additional differential wire pair, to transmitt the master clock. On software level, a plethora of synchronization techniques exist. More information on this issue can be found in [11].

##### Transmission Timing

Since every slave is connected to the master directly via RS-485, i.e. using UART ports of the MCUs connected to RS-485 driver modules, one needs to cycle through each transmission sequentially. Additionally, the same RS-485 connection is used for transmission and reception of the data, that is in half-duplex mode. During measurements, every time the master switches to the next slave and every time the half-duplex mode switches direction, a new transmission must be established, potentially introducing delay times.

These delays limit the overall data rate considerably and reduce the reliability of the system. It is advised to use a different approach, when increasing the sensor count. A daisy chain of all accelerometers in a full-duplex communication cycle, for example, enables the same connection to run continuously, where all slave devices append their respective sensor data to a long data string. Although more reliable, the physical layer of such a system must be carefully considered, since the total length of the wires increases by twice the distance between master and slave for every additional slave. Signal loss can only be prevented by adding signal repeaters or trough the use of higher supply voltages for the RS-485 transmission.

# 5

## Test Setups

The test conducted during this thesis isolated features of the prototype system described in Chapter 4. Measurement data has been compared to a reference system, called MODE3. Both systems are configured to include one impulse hammer, one DAC system and one three dimensional accelerometer, as well as a read out computer system with accompanying software.

### 5.1 System Costs

The difference in cost of the two system shows, why a low-cost system is desirable, if one is not interested in EMA of higher modes. Conventional EMA systems are manufactured for a small market compared to the low-cost sensors used in the prototype system. The price difference is significant. But this comes at the cost of lower lower resolution acceleration noise density in the case of the accelerometers and lower sensitivity as well as unknown frequency response in the case of the load cell.

The reference system represents a typical EMA measurement system, that typically consists of the following components:

- The LC, its charge amplifier and the impact hammer hardware
- A 3-axis accelerometer
- A signal channel analyzer that includes both signal conditioning and an ADC with the support for at least 4-channels
- Isolated cabling for analog signal transmission of all channels

Each of the listed points has an impact to the pricing of around 2500 swiss francs or more, giving an overall cost of the system of at least 10000 swiss francs.

In comparison, the sensors used in the prototype system cost approximately 5 respectively 80 swiss francs.

## 5.1 System Costs

Accelerometer	in system ...	Sensing element	Bandwidth / Hz	Dynamic range / g	Acceleration noise density / $\mu\text{g}/\sqrt{\text{Hz}}$	Estimated cost / CHF
PCB-356B18	MODE3	Piezoceramic	0.3...5000	$\pm 5$	1.2 (at 100 Hz)	3000
LIS3DSH	Prototype	Capacitive	1.5...800	$\pm 2/ \pm 4/ \pm 6/$ $\pm 8/ \pm 16$ (selectable)	150 (at 100 Hz and $\pm 2$ g)	5

**Table 5.1:** Accelerometer comparison. Note that MODE3 includes an enclosed accelerometer, whereas the MEMS accelerometer IC has been tested on an evaluation Printed Circuit Board (PCB).

Impact Hammer	in system ...	Sensing element	Frequency response / Hz	Range / kN	Sensitivity / $\mu\text{V/N}$	Estimated cost / CHF
IEPE Type 9726A2000	MODE3	Piezoceramic	5400	20	200	2500
Hammer with DYMH-103	Prototype	Strain gauge	unknown	3	3.3...5	250

**Table 5.2:** Impact hammer comparison. Note that the prototype system uses a strain gauge LC designed for weighting applications, whereas the MODE3 includes a closed impact hammer with an integrated piezoceramic.

Coupled with the fact, that no specially shielded cables are required for digital data transmission, and generally only low-cost components were used, the overall cost accumulated to approximately 800 swiss francs. Note that the prototype system is still missing casings and manufacturing costs.

The accelerometers used in the respective systems are compared in Table 5.1. If one sets the low-cost accelerometer to its smallest range, the acceleration noise density is still 100 times greater compared to the piezoceramic of the MODE3.

When comparing the LCs of the impact hammer the sensitivity is increased by a factor of 100 in favor of the reference system despite the fact that it covers almost seven times the range of the prototype system. The values can be compared in Table 5.2

The comparison of the ADCs of the two systems shows another key difference between the two. The MODE3 uses a dynamic signal analyzer, i.e. a module that integrates both signal conditioning of the analog inputs and digitization. It all of its channels in real-time. Each sensor of the MODE3 is connected to the module, therefore every signal is digitized by its high-resolution ADC. In the prototype system, the three accelerometer signals are conditioned and converted by the sensors internal circuit. Only the signal from the LC is digitized at the Aduino Due, which also acts as master device in the configuration shown in Figure 4.1a. A comparison of the different ADCs is listed in Table 5.3.

ADC	in system ...	Number of channels	A/D resolution / bit	Sample rate / S/s	Estimated cost / CHF
FOCUS II (Dynamic signal analyzer)	MODE3	4 (differential)	24	$2\dots 9.6 \times 10^4$	3000
Arduino Due	Prototype	12 (single-ended)	12	$0\dots 1 \times 10^6$	45
LIS3DSH	Prototype	3	16	3.125...1600	5

**Table 5.3:** ADC comparison. Note that the sample rate of the Arduino Due ADC can only be reached in optimal conditions, i.e. only one channel and ultra low software overhead. The FOCUS II and LIS3DSH ADC allow their respective maxima for all channels simultaneously.

## 5.2 Hammer-Hammer Test

The hammer tips of the impact hammers of both the prototype and the MODE3 system are hit against each other. The target of this test is to evaluate the signal quality of the LC in the prototype system.

We assume the force transmission from the point of impact to both load cells respectively to be lossless. Thus the recording accuracy of the prototype system is determined by the correlation of the two signal recordings.

The sampling rate of both systems is set to 1600 S/s. The components are shown in Figure 5.1. All hammer-hammer tests were conducted, using a DAC of form Figure 4.1a

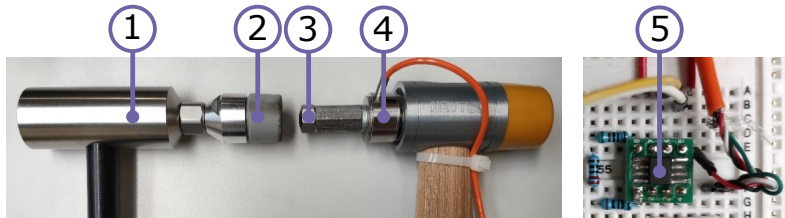


**Figure 5.1:** Hammer-Hammer test components

(1)	: Piezo + AMP!
(2)	: Soft Tip
(3)	: Tip 34CrMo4
(4)	: LC DYMH-103
(5)	: IN-AMP! AD627

**Table 5.4:** Legend to Figure 5.1

## 5.3 Andromeda Measurement

In the Andromeda measurement the accelerometers of both systems are positioned at close locations on the Andromeda test bench. Impact hammers of both the prototype and the reference system may be used as input signal. Because of this, the recording of the accelerometer signal of whichever system's impact hammer is not in use, is initiated before the impact and over a longer time frame. To compare signals of both systems, they are synchronized in the post analysis. The target of this test is to evaluate the signal quality of the accelerometer in the prototype system.

The Andromeda test bench consists of a wagon that is supported by a 3 m long linear drive in the x-axis on two 2.6 m apart, gantry y-axes that are linear drives as well. Hence kinematic chain

$$V[b[Y1Y2]X]$$

Figure 5.2 shows the test setup, while Figure 5.3 shows an example position of impact in the test setup.

The focus of this test is to compare the accelerometer signals. Therefore, we set the accelerometer parameter as defined in Table 5.5

Sensor Parameter	Sample Rate / Hz	Dynamic Range / g	Quantization / bit
Reference	1600	$\pm 5$	24
Prototype	1600	$\pm 4$	16

**Table 5.5:** Accelerometer parameter settings

#### 5.4 Filter Test Setups



**(a) Andromeda test setup**

**(b) Accelerometer view**

**Figure 5.2:** Andromeda test setup

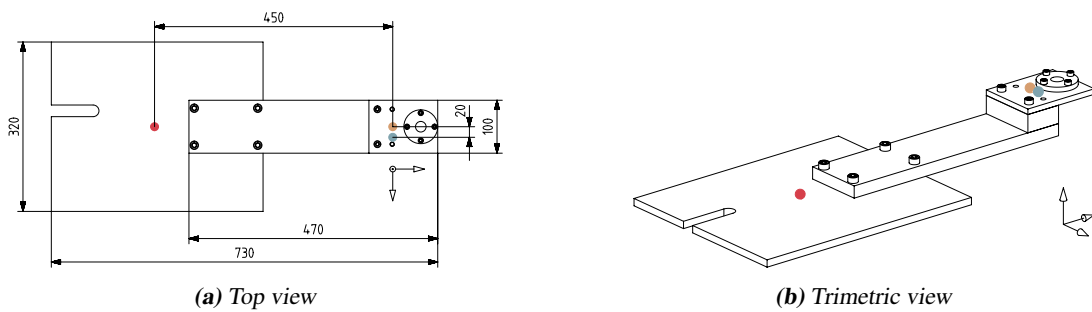


**Figure 5.3:** Andromeda wagon, example impact position

## 5.4 Filter Test Setups

The implementation of DAC setups as shown in Figure 4.1b required the testing of different filters. For this an Arduino script that allowed the analog-to-digital pins to output a differential sinusoidal signal. The filters then used the differential signal as input and the output was recorded onto the Arduino ADC for signal comparison. Different frequency inputs should verify the filters operation. Namely clock tunable filters, i.e. configurable cutoff frequency filters depending on the input frequency of a supply clock have been tested in this setup. For this a variable clock generator module has been used.

# 6

## Results and Discussion

In this chapter excerpt of the results using the above setups is presented.

### 6.1 Hammer-Hammer Test

The results of the hammer-hammer test are impulse signal recordings of both, the reference system and the prototype LC. Because the prototype signal is not calibrated, in order to able to compare the signals one needs to normalize the signal range of the reference signal. Furthermore, the signals need to be synced in time, by applying a time shift to one. The outputs gained after these transformations are shown in Figure 6.1.

It can be seen that if one is using the soft PVC tip of the reference system both signals correlate well. If we then focus on the detailed view of such a test, as seen in Figure 6.2, the difference in resolution becomes apparent.

### 6.2 Andromeda Measurement

Before comparing the accelerometer signals of the reference with the ones of the prototype system, one needs to subtract the constant gravitational part from the prototype signals. Additionally, the signals need to be synchronized in the time axis, as can be seen in Figure 6.3.

When we then consider the frequency domain of Figure 6.4 one can see that both signals cover the excited frequency bandwidth of around 250 Hz in a similar manner. The initial deviation at 1 Hz can be explained due to the signal conditioning in the reference system, where lower frequencies are cut-off.

## 6.2 Andromeda Measurement

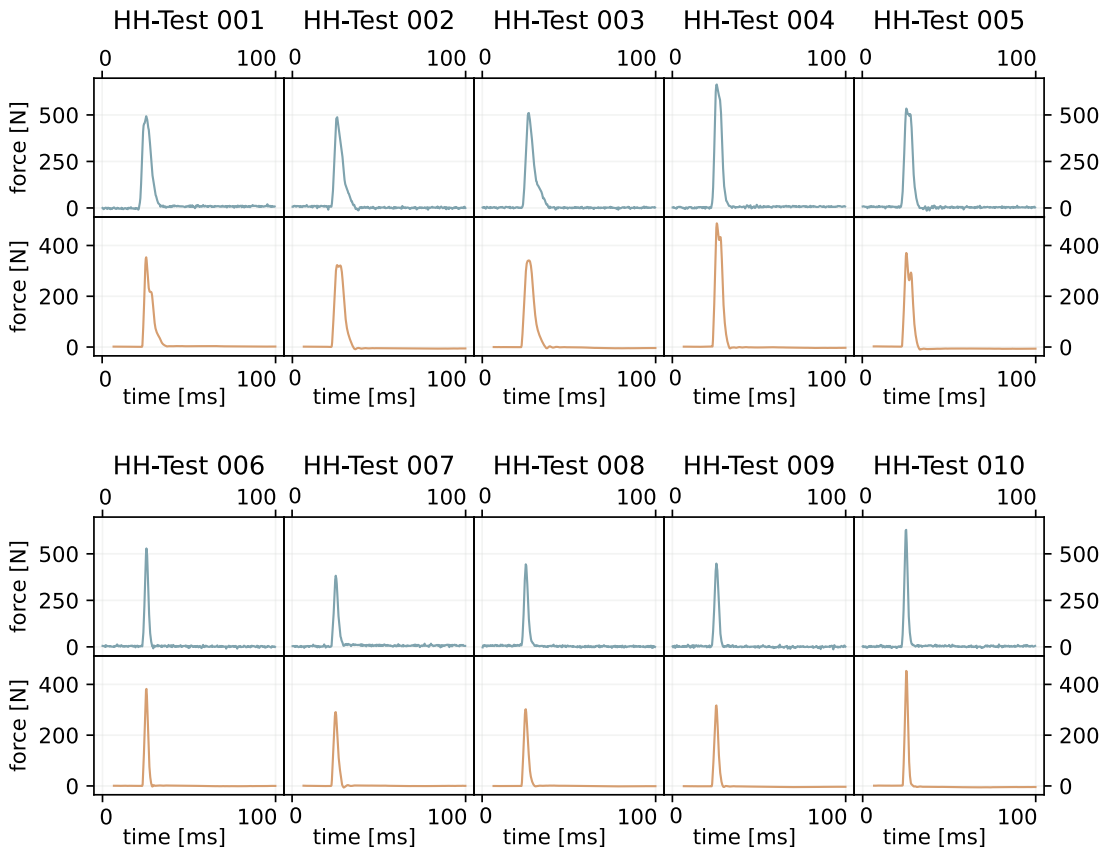


**Figure 6.1:** The HH-Test recordings of the reference hammer (orange) and the evaluated impact hammer system (turquoise). Note that the evaluated signal values are normalized so that the maxima are equal to the reference system.

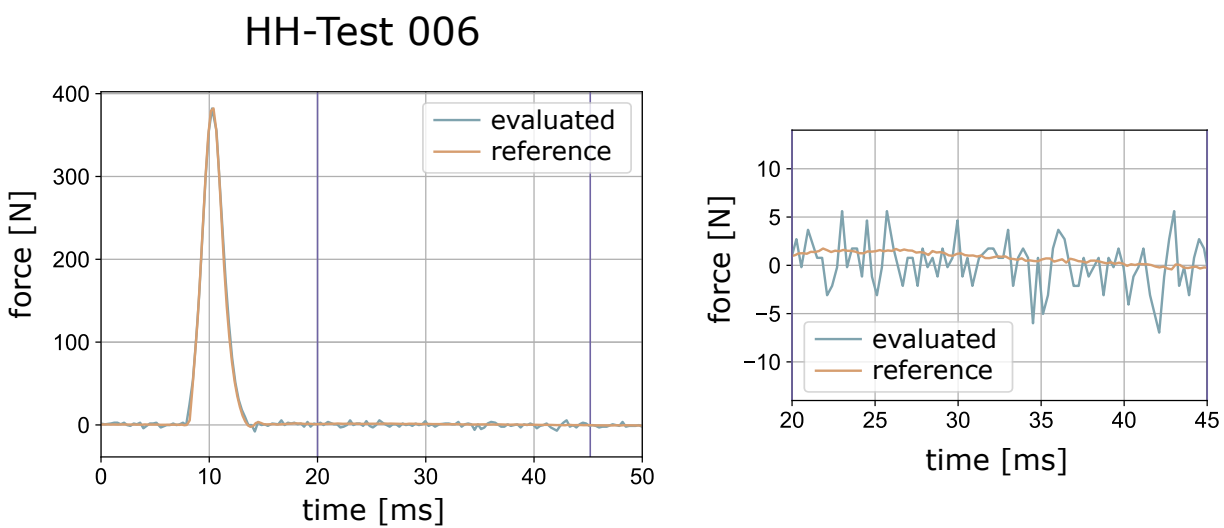


**Figure 6.2:** Detailed plot of HH-Test 006

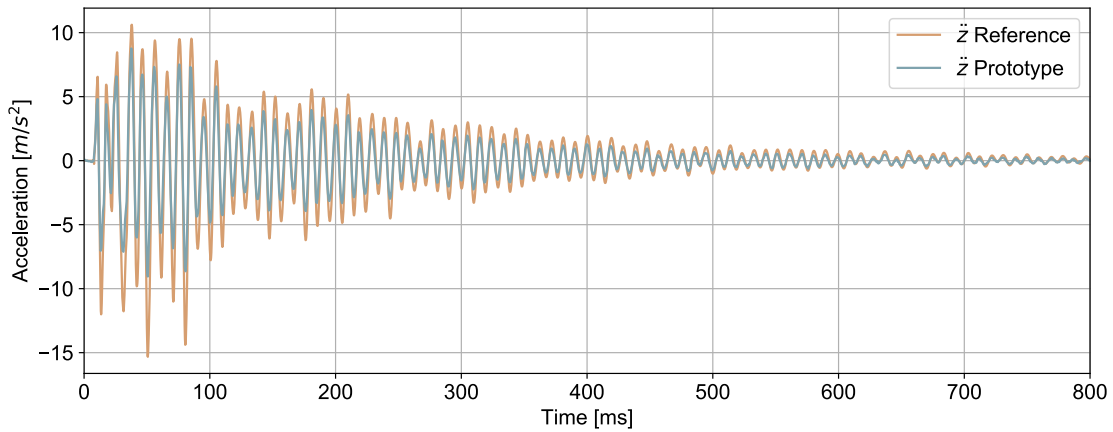


**Figure 6.3:** Measurement HAp024 in the time domain, excitation at point A, as shown in Figure 5.3

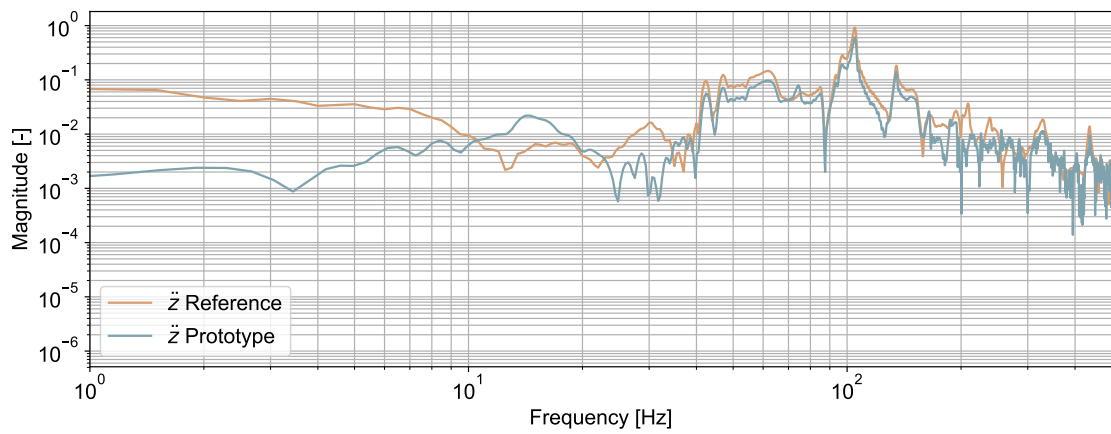


**Figure 6.4:** Measurement FFT HAp024, excitation at point A, as shown in Figure 5.3

## 6.3 Filter Test Setups

The implementation of Figure 4.1b is an iteration on the setup without a filter. But for the verification of the filter function a test setup was needed. But because of incompatibilities between the variable clock generator and the clock tunable filters, no meaningful output signals could be measured.

# 7

## Conclusion and Future Work

### 7.1 Conclusion

A force impact hammer has been constructed from only low-cost components. It has been demonstrated that a built in strain gauge load cell, which was designed for weighting applications, can follow the impulse trajectories with practically no overshoot. Said trajectory consistently follows the impulse of a reference piezoceramic apart from some expected increase in noise. The output signal of an experimental modal analysis measurement has been captured by a low-cost accelerometer which then showed a good correlation to a reference sensor. Furthermore, a microcontroller based data acquisition system has been developed with a specialized transmission protocol for microcontroller inter-communication. In this system, the use of a semi-duplex connections proved to decrease the reliability of the data acquisition.

### 7.2 Progress and Points of Transfer

Regarding the different layers of this project, it can be improved at multiples points. The filter has not been successfully implemented into the analog signal chain of the load cell yet. Neither were the clock tunable filters operational. As soon as the filter is integrated in the signal chain the upper bandwidth limit of the load cell can be tested with the use of harder hammer tips. The data flow of the data acquisition system did not prove to be sufficiently reliable. Before multi-channeling accelerometers, one needs to consider to change the dataflow, for example by enabling daisy-chaining of the accelerometers. One also can consider iterating the time synchronization.

## 7.3 Future Work

The low-cost modal analysis system is not finished as it is. Multi-Channeling the accelerometer, industrializing, and eventually miniaturizing the product are the key next steps in the development. Of course testing, evaluating and comparing signals to a reference system and models will play an important role in guaranteeing the systems accuracy. Additionally, one can improve on what already exists, as described in the previous section. In the same way, we can also exchange components, adding different features. For example a better real time capability by switching from Arduino to a Raspberry Pi or even field programmable gate arrays. It is also possible to switch to wireless communication between nodes or test the limits of the current data bandwidth.

Our ultimate goal is to reduce costs of the modal analysis measurement procedure. Apart from the development of this system it will also become increasingly important to address the software interface and generally the handling of the device. Because it should become possible, that the specialists do not have to conduct the measurements themselves. For this, we need to make the device accessible to anyone with the use of thorough instructions and/or increased automation.

# A

## Appendix

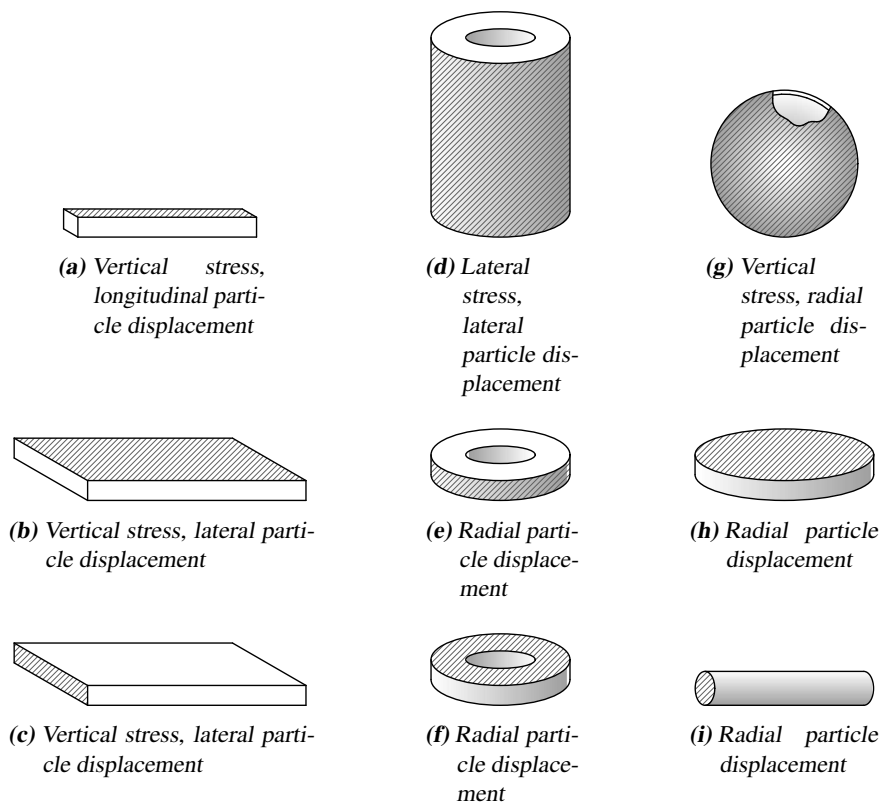


**Figure A.1:** Piezoelectric designs, where electrodes are placed on the shaded areas

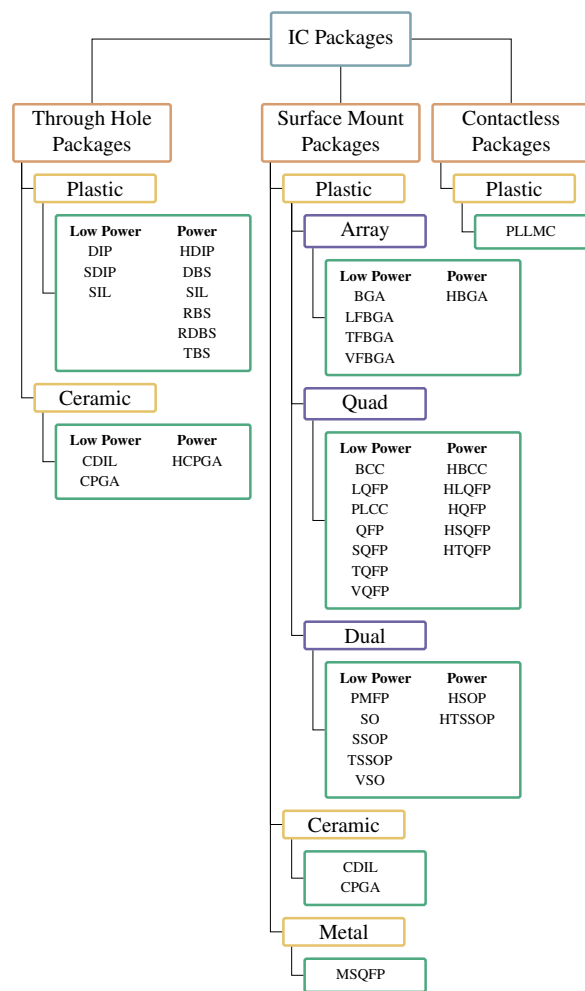


**Figure A.2:** Flowchart of IC packages

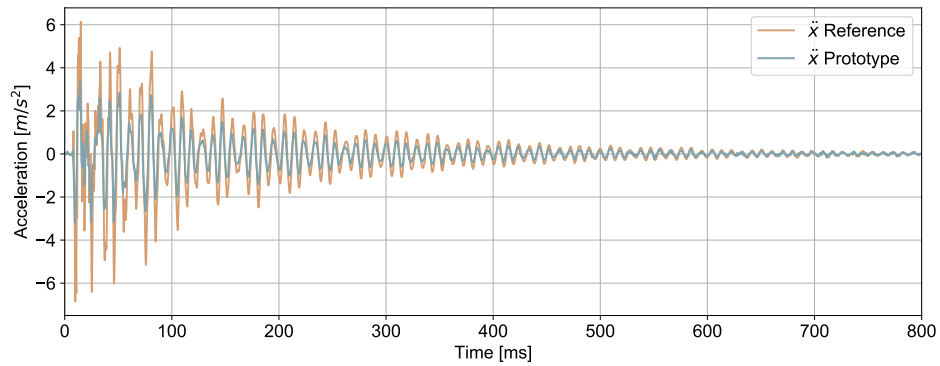


**Figure A.3:** Measurement HAp024 in the time domain, excitation at point A, as shown in Figure 5.3

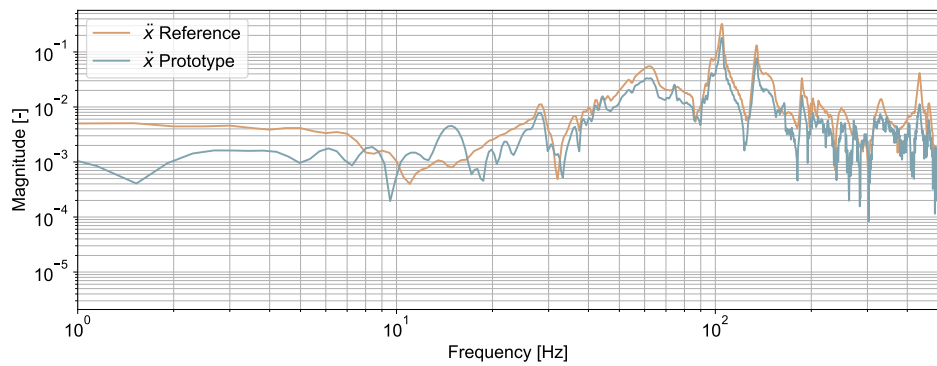


**Figure A.4:** Measurement FFT HAp024, excitation at point A, as shown in Figure 5.3

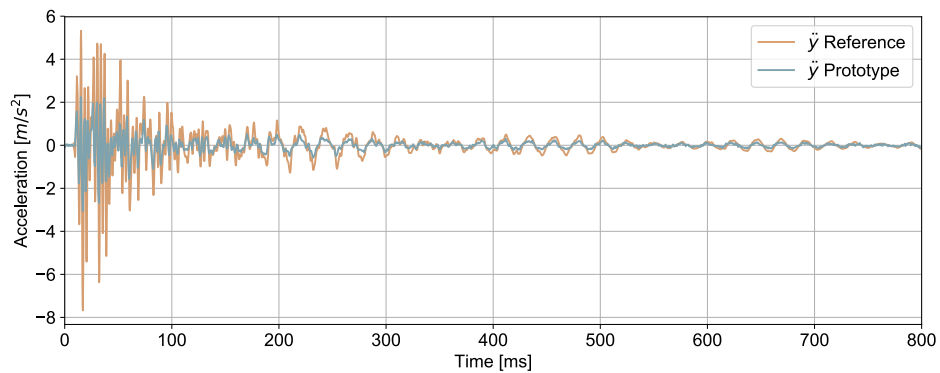


**Figure A.5:** Measurement HAp024 in the time domain, excitation at point A, as shown in Figure 5.3

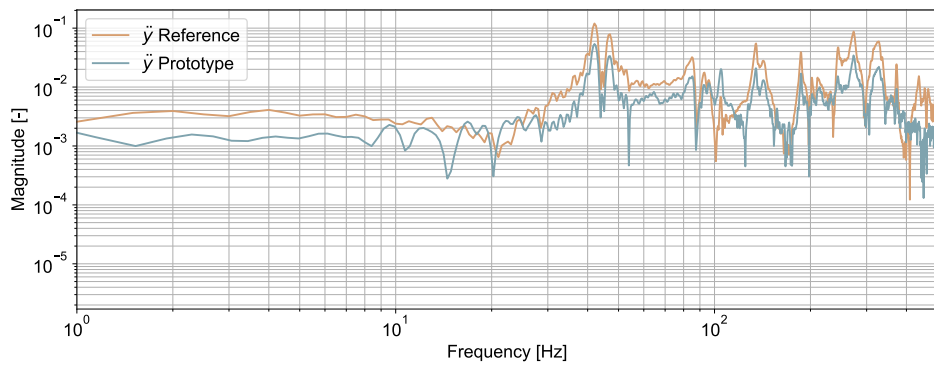


**Figure A.6:** Measurement FFT HAp024, excitation at point A, as shown in Figure 5.3

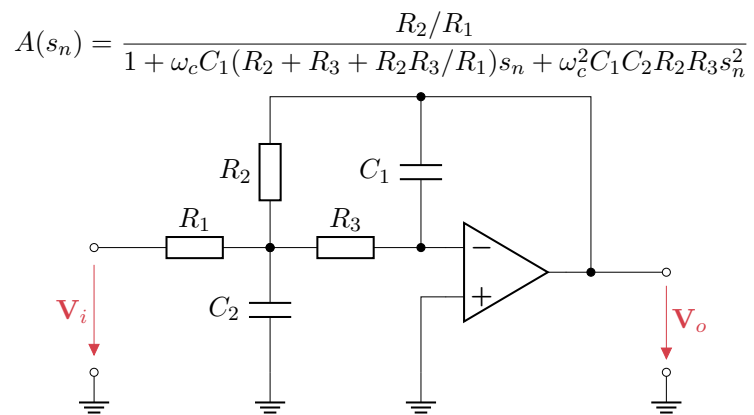


**Figure A.7:** Active second-order LPF with multiple negative feedback

# List of Figures

2.1	Digital Instrument . . . . .	3
2.2	Piezoelectric Accelerometer . . . . .	5
2.3	Second-Order System Bode Plots . . . . .	6
2.4	Strain Gauge . . . . .	7
2.5	Piezoelectric Sensors in Amplifier Circuits . . . . .	8
2.6	Capacitive Displacement Transducers . . . . .	9
2.7	Capacitive MEMS Accelerometer . . . . .	10
2.8	Forced Vibration Sources . . . . .	11
2.9	Frequency Response Measurement . . . . .	12
2.10	OSI Model . . . . .	15
2.11	SPI Bus Configurations . . . . .	16
3.1	Main OPA types . . . . .	19
3.2	Transfer characteristics of OPAs . . . . .	20
3.3	Controllability of VV-OPA signal outputs . . . . .	20
3.4	Equivalent Noise Bandwidth of an Amplifier . . . . .	22
3.5	Typical Instrumentation Amplifier Design . . . . .	23
3.6	Passive first-order LPF . . . . .	24
3.7	Passive second-order LPF . . . . .	26
3.8	LPF Pass- and Stopband . . . . .	28
3.9	Step response of fourth-order LPF . . . . .	28
3.10	Impulse response of fourth-order LPF . . . . .	29
3.11	Influence of LPF order $N$ on the amplitude of the frequency response . . . . .	30
3.12	Influence of the LPF order $N$ on the phase of the frequency response . . . . .	32
3.13	Influence of the LPF order $N$ on the group delay of the frequency response . . . . .	34
3.14	First-Order Lowpass Filter Topologies . . . . .	35
3.15	Active Second-Order LPF With Single Positive Feedback . . . . .	35
3.16	Aliasing . . . . .	36
3.17	ADC LSB waveform . . . . .	37
3.18	ADC thermal noise . . . . .	38

## *List of Figures*

4.1	DAC Building Blocks . . . . .	39
4.2	Data flow . . . . .	42
5.1	Hammer-Hammer Test components . . . . .	47
5.2	Andromeda Test Setup . . . . .	48
5.3	Andromeda Example Positions . . . . .	48
6.1	HH-Test comparison . . . . .	50
6.2	HH006 Plot . . . . .	50
6.3	Andromeda Measurement HAp024, Time Domain in Z-Axis . . . . .	51
6.4	Andromeda Measurement HAp024, FFT in Z-Axis . . . . .	51
A.1	Piezoelectric designs . . . . .	55
A.2	IC packages flowchart . . . . .	56
A.3	Andromeda Measurement HAp024, Time Domain in X-Axis . . . . .	57
A.4	Andromeda Measurement HAp024, FFT in X-Axis . . . . .	57
A.5	Andromeda Measurement HAp024, Time Domain in Y-Axis . . . . .	57
A.6	Andromeda Measurement HAp024, FFT in Y-Axis . . . . .	58
A.7	Active Second-Order LPF With Multiple Negative Feedback . . . . .	58

# List of Tables

2.1	Legend to Piezoelectric Accelerometer . . . . .	5
3.1	ADC Topologies . . . . .	38
4.1	Legend to DAC Building Blocks . . . . .	39
4.2	MCUs Used . . . . .	40
4.3	MCU Communication Protocol . . . . .	41
5.1	Accelerometer Comparison . . . . .	46
5.2	Impact Hammer Comparison . . . . .	46
5.3	ADC Comparison . . . . .	46
5.4	Legend to Hammer Hammer Test Components . . . . .	47
5.5	Set Accelerometer Parameters . . . . .	47



# Bibliography

- [1] Sherif Beskyroun and Q. Ma. “Low-cost accelerometers for experimental modal analysis”. In: *Proc. of the 15th World Conference on Earthquake Engineering*. 2012.
- [2] Bill Buchanan. *The Handbook of Data Communications and Networks: Volume 2*. Vol. 2. Springer Science & Business Media, 2004.
- [3] Yum Ji Chan and Jing-Wei Huang. “Multiple-point vibration testing with micro-electromechanical accelerometers and micro-controller unit”. In: *Mechatronics* 44 (2017), pp. 84–93.
- [4] Ozak O Esu et al. “Integration of low-cost consumer electronics for in-situ condition monitoring of wind turbine blades”. In: (2014).
- [5] Alberto Girolami et al. “Modal analysis of structures with low-cost embedded systems”. In: *2018 IEEE International Symposium on Circuits and Systems (ISCAS)*. IEEE. 2018, pp. 1–4.
- [6] C Hall, R Andrews, and J Wuerker. *Fundamentals of Precision ADC Noise Analysis*. Tech. rep. Texas Instruments, Incorporated, 2020.
- [7] C Kitchin and L Counts. *A Designer’s Guide to Instrumentation Amplifiers*. Tech. rep. Analog Devices, Incorporated, 2006.
- [8] Hein Marais. “RS-485/RS-422 circuit implementation guide”. In: *AN-960 Analog Devices* (2008).
- [9] Gianfranco Piana et al. “Experimental modal analysis of straight and curved slender beams by piezoelectric transducers”. In: *Meccanica* 51.11 (2016), pp. 2797–2811.
- [10] Brian J Schwarz and Mark H Richardson. “Experimental modal analysis”. In: *CSI Reliability week* 35.1 (1999), pp. 1–12.
- [11] Sundararajan Sriram and Shuvra S Bhattacharyya. *Embedded multiprocessors: Scheduling and synchronization*. CRC press, 2018.
- [12] Stiny. *Aktive elektronische Bauelemente*. Springer Fachmedien Wiesbaden, 2019.
- [13] Tietze. *Electronic Circuits*. Springer Berlin Heidelberg, 2008.
- [14] Josef Vollmer et al. “Construction kit for low-cost vibration analysis systems based on low-cost acceleration sensors”. In: *2009 IEEE/ASME International Conference on Advanced Intelligent Mechatronics*. IEEE. 2009, pp. 463–468.

## Bibliography

- [15] Chris Waltham and Andrzej Kotlicki. “Construction and calibration of an impact hammer”. In: *American Journal of Physics* 77.10 (2009), pp. 945–949.
- [16] Tong Wang et al. “Practical calibration techniques for the modal impact hammer”. In: *Sensors and Instrumentation, Volume 5*. Springer, 2015, pp. 23–29.
- [17] John G Webster and Halit Eren. *Measurement, Instrumentation, and Sensors Handbook: Two-Volume Set*. CRC press, 2018.
- [18] Arthur Williams. *Analog filter and circuit design handbook*. McGraw Hill Professional, 2014.